

# Microfluidics platform for studies of peptide – polyelectrolyte interaction

Marcus Wanselius<sup>a</sup>, Sean Searle<sup>a</sup>, Agnes Rodler<sup>a</sup>, Maria Tenje<sup>b</sup>, Susanna Abrahmsén-Alami<sup>c</sup>, Per Hansson<sup>a,\*</sup>

<sup>a</sup> Department of Medicinal Chemistry, Uppsala University, BMC P.O. Box 574, SE-751 23, Uppsala, Sweden

<sup>b</sup> Department of Material Science and Engineering, Science for Life Laboratory, Uppsala University, P.O. Box 35, SE-751 03 Uppsala, Sweden

<sup>c</sup> Innovation Strategies & External Liaison, Pharmaceutical Technology & Development, Operations, AstraZeneca, Gothenburg, Sweden

## ARTICLE INFO

### Keywords:

Microfluidics  
Microgel  
Subcutaneous administration  
*In vitro* method  
Polyelectrolyte  
Peptide  
Protein  
Drug

## ABSTRACT

Subcutaneous injection is one of the most common approaches for administering biopharmaceuticals unsuitable for oral delivery. However, there is a lack of methods to predict the behavior of biopharmaceuticals within the extracellular matrix of the subcutaneous tissue. In this work, we present a novel miniaturized microfluidic-based *in vitro* method able to investigate interactions between drug molecules and the polymers of the subcutaneous extracellular matrix. To validate the method, microgels consisting of, respectively, covalently cross-linked hyaluronic acid, polyacrylic acid, and commercially available DC Bead™, were exposed to three model substances: cytochrome C, protamine sulfate and amitriptyline hydrochloride. These components were chosen to include systems with widely different physiochemical properties (charge, size, self-assembly, etc.) The experimental results were compared with theoretical predictions from a gel model developed earlier. The results show that the method is suitable as a rapid screening method for automated, large-scale, probing of interactions between biopolymers and drug molecules, with small consumption of material.

## 1. Introduction

Subcutaneous injection is a common administration route for pharmaceutical peptides and proteins. However, while avoiding the significant difficulties associated with oral uptake, such as degradation in the digestive tract and first-pass metabolism, the faith of subcutaneously administered drugs is often difficult to predict (Kinnunen and Mørn, 2014; Patel et al., 2014; Richter et al., 2012; Richter and Jacobsen, 2014; Viola et al., 2018; Wu et al., 2013; Zou et al., 2021). For many drug products, the fraction of drug molecules reaching the circulatory system is low, and there is often significant variation between patients, which is a problem shared with oral delivery of macromolecules. Aggregation of the drug after injection and interaction with the extracellular matrix (ECM) constituents in the subcutaneous environment are factors believed to contribute to the limited bioavailability and poor absorption predictability. From this perspective, it is essential to investigate how drug candidates interact with the constituents of the ECM early in the drug development phase. In the present work, we describe and evaluate a microfluidic method for probing interactions based on the responsiveness of polyelectrolyte microgels to oppositely charged species. As responsive microgels are used as drug carriers in, e.g., trans arterial

chemoembolization (TACE) (Hagan et al., 2019), the method is also suitable for *in vitro* studies of microgel-based delivery systems.

Collagen, hyaluronic acid, and chondroitin sulfate are the major macromolecular species of the extracellular matrix in subcutaneous tissue (Kinnunen and Mørn, 2014). Collagen triple helices form a weakly charged, three-dimensional fiber network, primarily responsible for the mechanical rigidity of the tissue. The pores in the network are large enough not to sterically hinder the transport of small peptides, but can affect the mass transport of larger species like, e.g., antibodies (Kinnunen and Mørn, 2014; Wiig and Swartz, 2012). Hyaluronic acid and chondroitin sulfate are negatively charged glycosaminoglycans dissolved in the interstitial fluid between the collagen fibers. The highly charged chondroitin sulfate (~1 negative charge per 5 Å along the chain) is expected to interact electrostatically with net positively charged peptides, affecting their transport rate. Hyaluronic acid has a lower linear charge density (~1 negative charge per 10 Å) but is present at a higher concentration and may affect the transport properties to an even larger extent than chondroitin sulfate.

The interaction between proteins and hyaluronic acid and other biopolyelectrolytes has been studied extensively in the past (Cooper et al., 2005; Kayitmazer et al., 2013). There are also several examples of

\* Corresponding author.

E-mail address: [per.hansson@ilk.uu.se](mailto:per.hansson@ilk.uu.se) (P. Hansson).

<https://doi.org/10.1016/j.ijpharm.2022.121785>

Received 26 January 2022; Received in revised form 12 April 2022; Accepted 26 April 2022

Available online 30 April 2022

0378-5173/© 2022 The Authors. Published by Elsevier B.V. This is an open access article under the CC BY license (<http://creativecommons.org/licenses/by/4.0/>).

these interactions being utilized for protein or peptide formulation (Chan et al., 2007; Jones et al., 1997; Cui et al., 2005; Cadée et al., 2002; Kim et al., 2005; Koten et al., 2003). The results from several *in vitro* studies of mixtures of proteins and polyelectrolytes of opposite charge have revealed the importance of electrostatic interactions. Thus, complex formation and phase separation are generally favored by the high net charge of both species, low ionic strength, and high flexibility of the polyelectrolyte (de Kruif et al., 2004; de Vries and Cohen Stuart, 2006). However, the distribution of charges on the protein and charge regulation have also been shown to be important (Barroso da Silva et al., 2006). The latter properties have been proposed to explain why complex formation and even phase separation have been observed in mixtures of species of the same charge sign, sometimes described as complexation on the “wrong side” of the isoelectric point (de Kruif et al., 2004; Weinbreck et al., 2004). Many results have been obtained from phase studies through turbidimetric titration or analysis of the composition of co-existing phases in phase-separated samples, in combination with rheological and structural investigations.

Methods have been developed to help predict the behavior of subcutaneously injected molecules. Pion's Scissor system is an *in vitro* method for predicting the dissolution and absorption of drugs after administration (Kinnunen et al., 2015). The drug formulation of interest is injected into a solution based on high molecular weight hyaluronic acid in a cartridge, where diffusion and aggregation of the injected formulation can be monitored. HypoSkin® is an *ex vivo* method where whole skin tissue samples from abdominal surgery are preserved and placed in a biological matrix to keep the sample alive for at least 7 days (Pages et al., 2018). A drug formulation is injected into the subcutaneous layer of the tissue sample, and concentration measurements are made in a release medium below the skin tissue. Several *in vitro* methods utilize agarose or Sephadex® hydrogels aiming to mimic the subcutaneous tissue. These primarily mimic the pore structure found in the ECM but not the physicochemical interactions known to occur (Bock et al., 2020; Leung et al., 2017; Jensen et al., 2015; Jensen et al., 2016; Kožák et al., 2021).

The methods mentioned above have advantages and disadvantages, but they all typically require large amounts of material, not always available in investigations of drug candidates in the development phase due to cost and production possibilities. In our laboratory, we have developed microscopy techniques to investigate how proteins, peptides, and self-assembling amphiphiles interact with single polyelectrolyte microgels (Ahnfelt et al., 2018; Ahnfelt et al., 2016; Al-Tikriti and Hansson, 2020; Andersson and Hansson, 2018; Andersson et al., 2005; Bysell et al., 2008; Bysell et al., 2010; Bysell et al., 2010; Hansson, 2020; Hansson et al., 2012; Jidheden and Hansson, 2016; Johansson and Hansson, 2010; Johansson et al., 2009; Nilsson and Hansson, 2005; Nilsson and Hansson, 2007). The principle behind the techniques is that weakly cross-linked polyelectrolyte networks respond to the loading and release of oppositely charged drugs by changing their volume and internal morphology. The responsiveness results from the delicate balance between elastic forces in the network and the osmotic swelling forces sensitive to the concentration of network counterions inside the microgel (Hansson, 2020; Gernandt and Hansson, 2012). The exchange of a few percent of monovalent counterions for a charge equivalent amount of multivalent protein molecules is sufficient to give rise to a measurable volume change. The effect has been studied extensively with polyelectrolyte hydrogels of macroscopic size, investigations that have revealed many interesting features about the systems, such as volume-phase transitions and phase coexistence in gels (Kabanov et al., 2004; Zevin et al., 2002). We have shown that the same phenomena can also be studied by micropipette-assisted microscopy techniques by monitoring spherical microgels of 10 – 500 µm diameter (Hansson, 2020). The technique was pioneered by Needham and co-workers (Eichenbaum et al., 1999; Eichenbaum et al., 1999; Eichenbaum et al., 1998; Kiser et al., 1998), investigating the triggered release of doxorubicin from a lipid-coated microgel particle. Their studies showed that it is possible to

gain information about the internal distribution of material inside the microgels, which is essential for understanding the mechanisms of loading and release. Significant advantages with these types of miniaturized experiments are fast gel response and small consumption of material. Recent developments make it possible to measure also the amount of drug loaded onto a single microgel (Al-Tikriti and Hansson, 2020; Jidheden and Hansson, 2016). For kinetic studies, micromanipulators can be used to position single microgels in a liquid of controlled flow rate inside a flow-pipette. This has been used extensively to investigate loading/release of peptides (Bysell et al., 2008; Bysell et al., 2010; Bysell et al., 2010; Bysell and Malmsten, 2006; Bysell and Malmsten, 2009; Bysell et al., 2011; Bysell et al., 2009) and amphiphilic drugs (Ahnfelt et al., 2018; Al-Tikriti and Hansson, 2020) to/from microgels. Results thereof have been used to discriminate between particle- and film-controlled binding and release kinetics (Ahnfelt et al., 2018; Al-Tikriti and Hansson, 2020). A drawback is that it is difficult to measure directly the amount loaded or released. Instead, one must rely on models providing relationships between the gel volume and drug load (Nilsson and Hansson, 2005; Nilsson and Hansson, 2007; Gernandt and Hansson, 2012; Gernandt and Hansson, 2016; Hansson et al., 2002; Nilsson and Hansson, 2008). Furthermore, while the micropipette/micromanipulator approach is beneficial for detailed investigations of particular systems, it is quite cumbersome to use, and permits only the examination of one microgel at a time.

In the present work we have replaced the micropipette/flow pipette setup with an array of hydrodynamic microgel traps on a microfluidic chip to make the microgel method more efficient. Microfluidics has been used extensively to synthesize drug delivery particles and to study, *in vitro*, drug delivery in simulated physiological environments (Björnmalm et al., 2014). For our purpose, microfluidics has the advantage that it allows us to simultaneously monitor a large number of microgels in contact with the same liquid medium. Furthermore, it becomes easy to change the medium, and the material consumption is small, making the technique suitable for screening purposes. As a proof of concept, we have investigated, in this work, anionic microgel networks consisting of respectively covalently cross-linked hyaluronate (HA) and polyacrylate (PA), both synthesized in our lab. In addition, we have studied commercially available DC Bead™ containing poly(vinyl-alcohol) integrated with the negatively charged poly(2-acrylamido-2-methylpropanesulfonate) into one network. As model substances interacting with the microgels, we have investigated cytochrome C (Cyt C), a globular shaped protein of lower net charge at neutral pH (+7), protamine sulfate (PRO), which is a linear polypeptide of high charge density at pH 7.4 (+21 net charges), and amitriptyline hydrochloride (AMT), a cationic amphiphilic drug of net charge +1 at pH 7.4 known to form micelles in polyacrylate gels (Al-Tikriti and Hansson, 2020).

The purpose of the present paper is to demonstrate that the microfluidics-based method can be used to probe drug–polyelectrolyte interactions using small amounts of drug substance with opportunities to gain sufficient statistics for further data analysis. To evaluate the result, it is necessary to describe which type of information one expects from the method based on previous results from single-microgel experiments. To this end, we will compare the experimental results with the expected outcome from a theoretical gel model developed earlier (Jidheden and Hansson, 2016; Gernandt and Hansson, 2016; Andersson and Hansson, 2017), shown to capture semi-quantitatively the general features of the systems.

## 2. Materials and methods

### 2.1. Chemicals

Polydimethylsiloxane (PDMS) DowSyl Sylgard™ 184 was obtained as a kit including elastomer base and curing agent purchased from GA Lindberg ChemTech AB (Stockholm, SE). Picosurf™ 5% in Novec™ 7500 was acquired from Sphere fluidics (Cambridge, UK) and Novec™

7500 (greater than 99%) was purchased from 3 M (Saint Paul, MN, USA). Sodium hyaluronate (100–300 kDa) was purchased from Contipro a.s. (Dolní Dobrouč, CZ) and DC Bead™ (will further on be denoted as DC bead) (70–150 µm) from Biocompatibles UK Ltd (Surrey, UK). The linker N-(2-aminoethyl) acrylamide hydrochloride (AEA) was from abcr GmbH (Karlsruhe, GE), and Spectra/Por® 6 RC-membrane (3.5 kDa cutoff) was from SpectrumLabs (Rancho Dominguez, CA). SUEX photoresist film was from DJ MicroLaminates (Sudbury, MA, USA) 2-propanol (ACS reagent) was purchased from Merck KGaA (Darmstadt, GE) and Ethanol (99.7%) was from Solveco (Rosersberg, SE). EDC (N-(3-dimethylaminopropyl)-N'-ethylcarbodiimide hydrochloride) was acquired from Acros Organics, (Geel, BE). mr-Dev 600 development solution was from micro resist technology GmbH (Berlin, GE). Acrylic acid (anhydrous 99%), N,N,N',N'-tetramethylethylenediamine (TEMED) (ReagentPlus 99%), N,N'-methylenebisacrylamide (99%), ammonium persulfate (powder ≥ 98%), sodium phosphate monobasic (ReagentPlus ≥ 99%), sodium phosphate dibasic (ReagentPlus ≥ 99%), sorbitane monostearate (Span 60, S7010), amitriptyline hydrochloride (A8404), protamine sulfate (P3369), cytochrome C from equine heart (C2506), lithium phenyl-2,4,6-trimethylbenzoylphosphinate (LAP, 900889), Sigmacote®, sodium chloride (NaCl, ≥ 99%), sodium hydroxide (NaOH, ≥ 97%), HOBt (1-hydroxybenzotriazole hydrate) (≥ 97.0%) and Acetonitrile (anhydrous 99.8%) were all purchased from Sigma Aldrich, SE. All aqueous solutions were prepared with deionized (DI) water (Millipore Synergy with UV ultrapure, type 1, water purification system, 18.2 MΩ cm at 25 °C, USA).

The standard aqueous medium in the microfluidic experiments contained 3.5 mM sodium phosphate monobasic and 1.5 mM sodium phosphate dibasic as buffer system. The pH was adjusted to 7.4 or 5.9 by adding small amounts of HCl, and the ionic strength was adjusted by adding NaCl. We will refer to phosphate buffered media of pH 7.4 and pH 5.9 as PB (pH 7.4) and PB (pH 5.9), respectively. The change in pH after dissolving the drug substances was 0.2 or less in all systems. A pH change of that magnitude in the studied pH range has no effect on the charge of the investigated molecules, showing that the buffer capacity of the medium was sufficient for the present purposes.

## 2.2. Microfluidic chip fabrication

The fabrication of microfluidic chips used in this work was done with standard soft lithography techniques (Duffy et al., 1998). Masters for the microfluidic chips were produced by first laminating a rinsed 4-inch silicon wafer with a 210 µm thick SUEX photoresist film. The lamination was performed at 60 °C followed by 5 min post-lamination bake at 80 °C. The laminated wafer was exposed to UV-light (wavelength 365 nm) in eight cycles of 30 s with 45 s cooling in between each cycle through a Cr/glass mask corresponding to the inverse of the microfluidic chip design. Afterwards, the exposed structures were left at 80 °C for another 3 h followed by cooling overnight. Finally, the non-crosslinked laminate was removed with a developer solution (mr-dev 600 from micro resist technology GmbH) for 60 min, with a solution renewal after 45 min. The development was stopped by rinsing the wafer with 2-propanol, and the master was examined for damages.

The microfluidic chips were made of PDMS, starting with mixing the base and curing agent in a 10:1 ratio, and cast over the master in a 14 cm petri dish. Vacuum was used to remove bubbles, and the PDMS was cured for 1 h at 70 °C. After curing, we peeled the PDMS from the master, cut it with a scalpel, and punched holes of diameter 0.75 mm for inlets and outlets. Cut PDMS structures were then covalently bonded to a glass slide after both were treated with air plasma for 30 s. After plasma treatment, both pieces were immediately put in contact, followed by 1 h in an oven at 70 °C. The chip used to produce hyaluronic acid-acrylamide microgels was further treated with Sigmacote® to render the channels hydrophobic. The chip was left to dry in the oven at 80 °C for 1 h.

Illustrations of the microfluidic chips for droplet production (MDP)

and interaction studies (MIS) can be seen in Figs. 1 and 2, respectively.

## 2.3. Microgel fabrication

Acrylamide-modified hyaluronic acid microgels (HA), and polyacrylic acid (PA) microgels were produced in-house. The production of PA microgels has been described elsewhere (Al-Tikriti and Hansson, 2020; Jidheden and Hansson, 2016; Wang et al., 1997). First, 2.6 g of acrylic acid, 11 g of 2 M NaOH (aq), 6.5 g of 80 mM linker N,N-methylenebisacrylamide, and 109 µL of TEMED were mixed with DI water to a total volume of 20 mL. Separately, 0.09 g of sorbitane monostearate was dissolved in 30 mL cyclohexane for 2 days with stirring. The sorbitane monostearate solution was heated to 45 °C and kept under a nitrogen atmosphere at 400 rpm stirring. Finally, 364 µL of 0.18 M ammonium persulfate was added to 10 mL of the reaction mixture, which immediately after was injected into the sorbitane monostearate solution. The temperature of the emulsion was increased to 60 °C. After stirring at 1000 rpm for 30 min, 40 mL of ethanol was added to break the emulsion. The ethanol/water phase containing microgels was transferred to a beaker and mixed with an excess of methanol. After mixing, the methanol phase was removed, and the microgel slurry was dried at 60 °C. After drying, the microgels were re-suspended in DI water and rinsed 4 times with DI water; pH was adjusted to above 9 by adding small aliquots of NaOH solution to keep the microgels stable.

The production of HA microgels was based on a protocol described previously (Porras Hernández et al., 2020; Shi et al., Mater 2017). Sodium hyaluronate was first functionalized by converting carboxylate groups into acrylamide groups. Briefly, 400 mg sodium hyaluronate were dissolved in 50 mL DI water together with the linker AEA (105 mg); the solution was kept in the dark. HOBt (152 mg) was dissolved separately in a 1:1 DI water/acetonitrile mixture during gentle heating. After cooling, the HOBt solution was added to the reaction mixture, and the pH was adjusted to 6 with 1 M HCl. Then EDC (287 mg) was added, and the reaction mixture was stirred for 24 h at room temperature. The mixture was dialyzed (Spectra/Por™ 3.5 kDa membrane) against 0.6% (w/v) NaCl (aq) solution at pH 3.5 for 24 h, then twice against DI water with pH adjusted to 3.5 for 24 h, followed by pure DI water. After dialysis, the reaction mixture was adjusted to pH 7 with NaOH, filtered (5 µm VDF, Millex Sterile Syringe Filters, Merck Millipore, Burlington, MA), and freeze-dried for 4–5 days. Purity and degree of modification were determined by <sup>1</sup>H NMR in D<sub>2</sub>O, indicating that 21% of disaccharide units were modified.

HA microgels were produced by utilizing a droplet-making chip of flow-focusing design (Fig. 1) and a OBK Mill + pressure pump with MFS flow sensors all from Elveflow (Elvesys, Paris, FR). Freeze-dried acrylamide modified HA was dissolved in a 0.1 % (w/w) solution of the photoinitiator LAP in DI water at a concentration of 2% (w/w); dissolution was done overnight at room temperature. A mixture of Novec™ 7500 with 0.5% (v/v) Picosurf™ was prepared and used as the continuous phase. The two solutions were transferred to Falcon tubes and connected to the droplet-making chip using tubing from Cole Parmer (Masterflex EW-06417–11) with an inner diameter of 300 µm. Flow rates were set to 5 µL/min and 120 µL/min for the aqueous and oil phase, respectively. Droplets were collected into a glass beaker and cross-linked using a UVP crosslinker CL-1000 from Analytik Jena, using UV-light of wavelength 365 nm and irradiation energy of 1000 µJ/cm<sup>2</sup> for 10 min. The emulsion was filtered through a 70 µm filter 3–10 times with DI water until oil and surfactant were washed away. The microgels were then re-suspended in PB (pH 7.4) and stored in the refrigerator.

## 2.4. Determination of microgel volume

Microgel volumes were determined from the diameter of each microgel. Images of the microgels were obtained with an Olympus BX51 microscope equipped with an UPlanFI 5 × lens and connected to an Olympus DP73 digital camera. Diameter measurements were achieved

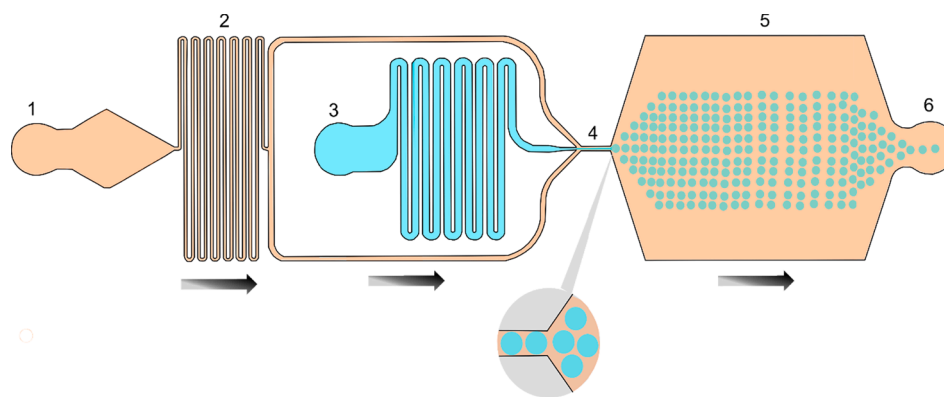


**Fig. 1.** Schematic (not according to scale) of microchip for droplet production (MDP); arrows indicate flow direction. (1) Inlet for oil phase (Novec™ 7500 0.5% Picosurf), (2) resistance to stabilize flow, (3) inlet for water phase (HA in DI water), (4) flow focus point where droplets are created, (5) observation chamber where flow rate is slowed down and size of w/o droplets can be examined, (6) outlet.

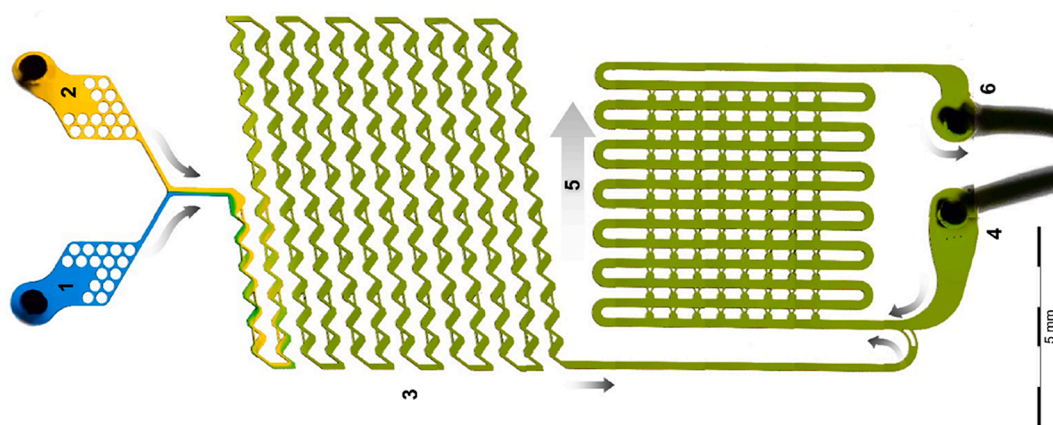


**Fig. 2.** Picture of a microfluidic chip used for interaction studies (MIS) taken during an experiment; arrows indicate the flow direction. (1) Inlet for solvent, (2) inlet for stock solution of drug molecule, (3) mixer for complete mixing of the solvent and stock solution, (4) inlet for microgels, (5) 96 single-microgel traps of 200 μm diameter, (6) outlet for liquid.

with the imaging software cellSens Dimension version 1.7.1 from Olympus Corporation.

### 2.5. Interaction experiments

The MIS shown in Fig. 2 and the OBK Mill + pressure pump with MFS flow sensors was used for all interaction experiments. Two tubings (Masterflex EW-06417–11) of inner diameter 300 μm were connected to the microfluidic chip via flow sensors, used to control the flow rate via the Elveflow smart interface software. A solution with an appropriate concentration (250 μM for PRO and Cyt C or 63.7 mM for AMT) of the substance under study in PB (pH 7.4 or 5.9) was pumped into the chip through one of the tubings (inlet 1) and PB (pH 7.4 or 5.9) without substance was injected through the other (inlet 2). By varying the flow rates of the two solutions, different concentrations could be acquired in the chip in a facile manner without manually changing solutions. At the start of each experiment, the chip was flushed with PB (pH 7.4 or 5.9) before loading the traps with microgels using a syringe connected via a piece of tubing to inlet 3. When the microgels were in the traps (200 μm in diameter), the flow rates of inlet 1 and 2 were modified to get the desired concentration of drug substance perfusing the trapped microgels. The volume flow rate through the chip was set at 200 μL/min if nothing else is specified. The corresponding apparent flow velocity through the traps was determined as  $12 \pm 2$  cm/s by using response rates of a model system measured with the micropipette method as a reference, as described in supplementary materials S1. The flow was in a

range where the swelling of the studied microgels was insensitive to variations of the flow rate (supplementary material S2).

### 3. Physicochemical properties of microgels and drug substances

Table 1 shows charge concentration, separation of charges along the polyelectrolyte chains (*b*), and radius of the microgels used; all data correspond to microgels in PB (pH 7.4). The microgels were chosen to cover a range of properties. PA microgels consist of covalently cross-linked sodium polyacrylate with flexible, highly charged chains that mainly interact electrostatically with proteins and micelles. HA microgels are made of covalently cross-linked acrylamide modified sodium hyaluronate chains. The HA backbone is fairly hydrophilic but bulkier and less flexible than PA. The *b* value given in Table 1 was calculated

**Table 1**  
Microgel properties. Charge concentration ( $C_0$ ) and linear separation of charges along the polyelectrolyte (*b*) and radius in PB (pH 7.4).

Microgel	Charge concentration, $C_0$ (mM)	Separation of charges, <i>b</i> (Å)	Microgel radius (μm)
PA microgel	90 (Al-Tikriti and Hansson, 2020)	2.5	75–85
DC bead	60 (Ahnfelt et al., 2018)	2.5 (PAMPS)	65–95
HA microgel	$15 \pm 5$	18 <sup>a</sup>	75–80

<sup>a</sup> Methacrylate modified HA (21% modification degree).

considering that 21 % of the carboxylate groups are modified by the cross-linker (see above). The linear charge density is thus considerably lower for HA than for PA, which explains the low charge concentration in the microgel. DC beads consist of uncharged polyvinyl alcohol (PVA) chains cross-linked with negatively charged poly(2-acrylamido-2-methylpropanesulfonate) chains (PAMPS) (Lewis et al., 2007). The linear charge density of PAMPS is the same as for PA, and both are expected to interact stronger with proteins and micelles than HA. However, the contribution to the osmotic pressure from the PVA chains prevents the network from collapsing to the same extent as PA networks upon loading of proteins and micelles. The large molecular weight per charge for HA is expected to play a similar role as PVA in DC beads (Hansson, 2009).

Table 2 shows the net charge and size of the three drug model substances. We have chosen Cyt C as a model representing globular proteins. Previous investigations show that the net charge is enough to associate it with negatively charged polyelectrolytes at moderate ionic strength but not large enough to induce volume phase transition in PA networks (Jidheden and Hansson, 2016; Johansson and Hansson, 2010). Furthermore, its propensity to self-associate is small. PRO was chosen as a model of a highly charged peptide drug. The biological function of this linear peptide is to condense DNA in sperm heads, but it is known to associate very strongly with other negatively charged polyelectrolytes (Zezin et al., 2002; Karabanova et al., 1995). AMT is used as a model of self-assembling drug. Previous studies show that AMT micelles associate with negatively charged polyelectrolytes and induce volume phase transition in PA networks (Al-Tikriti and Hansson, 2020) and DC bead (Ahnfelt et al., 2018). The size of the micelles is similar to that of a Cyt C molecule, but the net charge is higher, making them suitable for comparing charge effects. The micelle size in aqueous solutions was recently determined with small-angle x-ray scattering (Efthymiou et al., 2021). The data for AMT in Table 2 are representative of concentrated AMT solutions, comparable to the concentration inside fully loaded microgels.

#### 4. Gel theory

The size of polymer coils depends on the properties of the solvent and interactions with other species present in the solution. Flexible polyelectrolytes such as HA, PA, and PAMPS are particularly sensitive to the presence of molecules of opposite charge to the polyion chains (Cooper et al., 2005; de Vries and Cohen Stuart, 2006). When the chains are cross-linked to form three-dimensional networks such as microgels, the interactions affect the osmotic swelling of the network (Gernandt and Hansson, 2012; Gernandt and Hansson, 2016; Hansson, 2006). Recent work shows that it is possible to relate the magnitude of the volume response to the nature and strength of the interaction and, therefore, to the properties of the interacting species (Hansson, 2020; Gernandt and Hansson, 2015). The method presented in this work is based on that principle. To evaluate the performance of our microfluidics setup, we

**Table 2**

Drug properties. Charged groups per unit area, molecular weight, unit charges per molecule, and size.

Drug substance	Charged groups per unit area <sup>a</sup>	Molecular weight	Charge number <sup>a</sup>	Size
AMT micelle <sup>b</sup>	0.010 Å <sup>-2</sup>	11 kDa	+40	28x37x37 Å <sup>3</sup>
PRO (linear)	0.20 Å <sup>-1c</sup>	4.25 kDa	+21	~18 nm <sup>d</sup> (length)
Cyt C	0.0025 Å <sup>-2</sup>	12.3 kDa	+7	25x25x37 Å <sup>3</sup>

<sup>c</sup> Charged groups per unit length of stretched peptide chain.

<sup>a</sup> In PB (pH 7.4).

<sup>b</sup> Values for oblate shaped micelles of AMT with aggregation number 40 (Efthymiou et al., 2021).

<sup>d</sup> Estimated from an average length of 3.5 Å per amino acid in the peptide.

compared the experimental results with theoretical model calculations. The model, described in supplementary material S3, has been shown to account for many effects observed when polyelectrolyte gels interact with proteins (Jidheden and Hansson, 2016; Gernandt and Hansson, 2012) peptides (Hansson et al., 2012) self-assembling amphiphiles (Al-Tikriti and Hansson, 2020; Gernandt and Hansson, 2015, 2016) and multivalent ions (Hansson et al., 2012) both in systems of macrogels (~1 mL) and for spherical microgels in the size range used here. The topic was recently reviewed (Hansson, 2020). The model provides a relationship between the measured thermodynamic property (microgel volume) and the molecular interactions and can thus be used as a tool for data analysis to extract quantitative information about interactions (Gernandt and Hansson, 2012; Gernandt and Hansson, 2016).

For the purpose of this work, it is sufficient to consider the interaction between spherical drug proteins/micelles of positive charge and networks of flexible polyion chains of negative charge in the presence of monovalent salt ions and water. The mobile species are assumed to mix ideally, and the model corrects for the excluded volume interaction among the spheres. The Wall theory of rubber elasticity (Wall and Flory, 1951) describes the elastic free energy of the network. The spheres are defined by their radius  $r_s$  and charge number  $Z$ . The network is described by the elasticity parameter  $p$  related to the number of chain segments between cross-links, the concentration of segments  $C_p^*$  in a relaxed reference state of the network, and the fraction of charged segments  $q$ . The contribution of the chains to the gel volume is neglected, as is the volume of the small ions. The spheres interact via electric double layer forces. The electrostatic (free) energy is calculated using a cell model (Fig. 3A), taking into account ion-ion correlation effects in a simple but efficient way. This gives rise to an attraction between the spheres mediated by the network chains. For highly charged species, the attraction can lead to a phase transition, which for microgels in contact with a solution reservoir promotes massive binding accompanied by a collapse of the gel network at a critical concentration in the solution (Fig. 3B; left). During the transition, the “new” phase often forms a shell outside the “old” phase. The volume decreases gradually with increasing concentration for weakly charged species, and the gels are homogeneous at each loading level (Fig. 3B; right). In agreement with the experimental situation in the microfluidics setup, all theoretical calculations presented assume gels in contact with an infinite volume of an aqueous solution of monovalent salt at a concentration  $C_{salt}$  and spheres at concentration  $C_s$ .

#### 5. Results and discussion

##### 5.1. Microgels on a chip

Below we will demonstrate that valuable information about the interaction between macromolecular drugs and polyelectrolytes can be obtained from microfluidics studies of polyelectrolyte microgels. Fig. 4 shows microscopy images of the type of microfluidic chip used in this work with microgels positioned in the traps. The pictures were taken before (left panel) and after (right panel) the microgels had been exposed to drug solutions. Fig. 4A and 4B show DC beads interacting with Cyt C in PB (pH 7.4). In Fig. 4C and 4D, the experiment was repeated with PRO under the same conditions. Clearly, PRO gave rise to a larger volume decrease than Cyt C. Fig. 4E and 4F show that the interaction with AMT in PB (pH 5.9) leads to a dramatic volume collapse of HA microgels. Observations of this type can be quantified and used to extract valuable information about the strength of the interaction between charged species, including drugs and polyelectrolytes. In the subsequent sections, we will first show how to characterize the inherent responsiveness of the microgel networks, followed by a description of different types of interaction studies. Results from an investigation of the mass transfer rate to the microgels in the microfluidic traps show that conditions were comparable to those in the micromanipulator setup

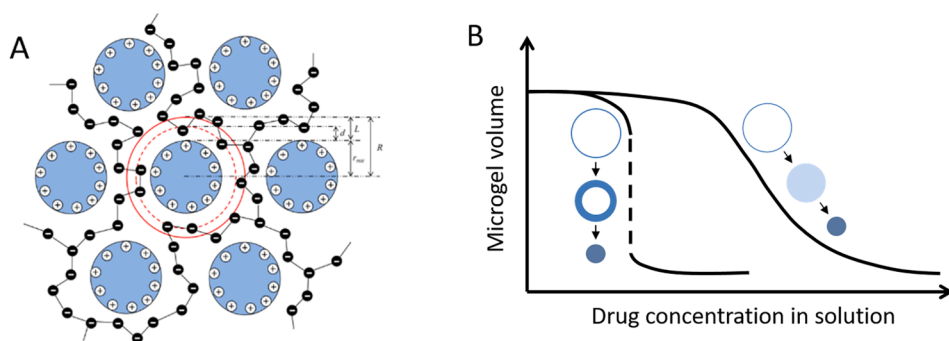


**Fig. 3.** A: Schematic drawing of charged spheres separated by a solution of cross-linked polyelectrolyte chains indicating the spherical cell of radius  $R$  used to calculate the electrostatic free energy in the model. Adapted from ref. (Hansson, 2009). B: Schematic plot of the gel volume response to drug concentration in the solution at high (left) electrostatic coupling between drug and microgel network (volume phase transition), and low (right) electrostatic coupling (continuous volume change). Adapted from ref. (Gernandt and Hansson, 2016).

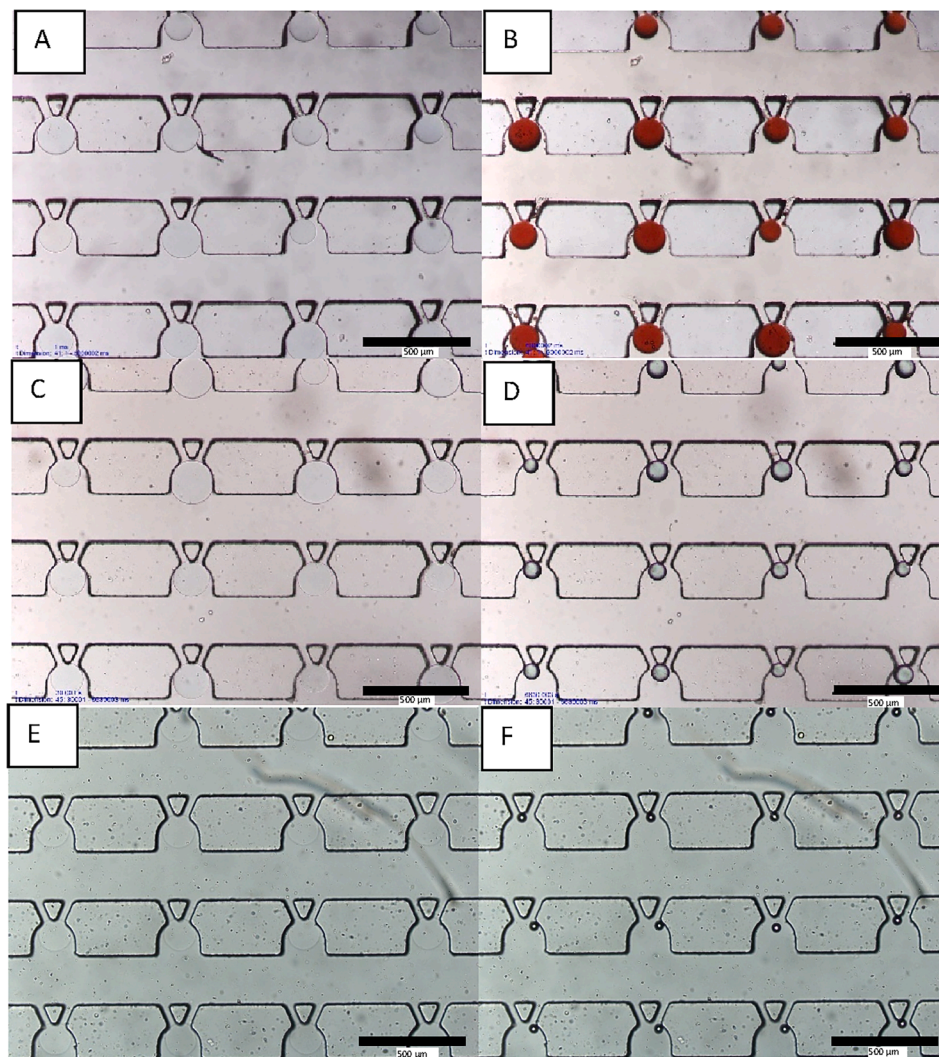


**Fig. 4.** Microgels in traps of the MIS. (A) DC beads in PB (pH 7.4) (B) same DC beads from picture (A) fully loaded with Cyt C. (C) DC beads in PB (pH 7.4), (D) same DC beads from picture (C) fully loaded with PRO. (E) HA microgels in PB (pH = 5.9), (F) same HA microgels from picture (E) fully loaded with AMT. Scale bar is 500 μm.

used earlier and that the confinement to the trap did not affect the swelling properties (supplementary material S1).

## 5.2. Characterization of microgel networks: Osmotic stress

For a given type of polyelectrolyte, both elasticity of the network and electrostatic coupling between the drug and the network determine the magnitude of the volume response (Hansson et al., 2012; Gernandt and

Hansson, 2012; Gernandt and Hansson, 2016). To be able to extract information about the latter, it is essential to characterize the former in the absence of a drug. This can be done by exposing the microgel to osmotic stress. A convenient method is to monitor the volume response to variation of the salt concentration in the solution. Fig. 5 shows the volume response of the microgels of the present study to increasing concentrations of NaCl in PB (pH 7.4). The ordinate shows the actual microgel volume  $V$  divided by the volume  $V_0$  in the reference medium

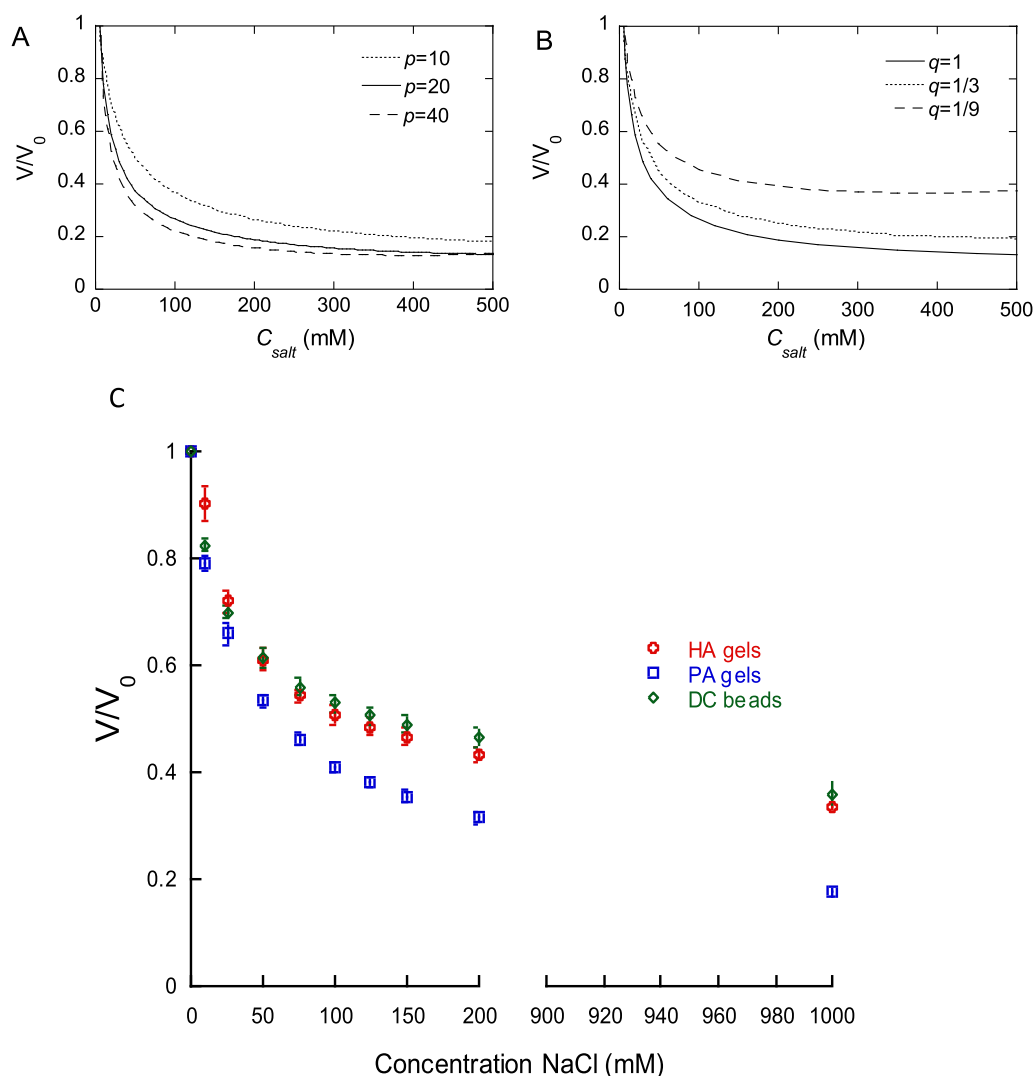


**Fig. 5.** Swelling of microgel networks as a function of monovalent salt concentration in the solution ( $C_{salt}$ ). A: Impact of network elasticity parameter ( $p$ ) as indicated. B: Impact of the fraction of charged network segments ( $q$ ). C: Experimental swelling of microgels (average of 8 microgels). Swelling is expressed as the volume ( $V$ ) ratio relative to the volume in PB (pH 7.4) ( $V_0$ ).

PB (pH 7.4). Fig. 5A-B shows theoretically calculated response curves for networks with different values of the elasticity parameter  $p$  (5A) and a fraction of charged segments in the polyelectrolyte chains  $q$  (5B). The former can be interpreted as the apparent number of chain segments between cross-links, a number decreasing with increasing degree of cross-linking of the network chains. In the model, the osmotic swelling forces are balanced by the contractive elastic forces in the network. The former is primarily determined by the difference in mobile ion concentration between the microgel and the liquid. According to theory, the deswelling produced by adding salt increases with both increasing  $p$  and  $q$ . The difference in experimental volume response between the HA and PA networks exposed to different NaCl concentrations (Fig. 5C) could thus result from both different degrees of crosslinking and linear charge density of the chains. In DC beads, the PAMPS component has the same linear charge density as PA, but a substantial part of the network consists of uncharged PVA chains. It is likely that the additional swelling pressure from the PVA chains contributes to the difference between DC beads and PA, but there could also be a difference in the degree of cross-linking.

For all three microgels, the deswelling effect per amount of added salt is largest at a low salt concentration where only small amounts of salt enter the microgel (Donnan effect). In the model, this is purely an effect of the decreased swelling pressure in the microgel due to the

increased osmotic pressure in the solution, allowing the network to relax to a state of lower elastic energy. The effect of increasing the salt concentration was small for concentrations above 100 mM. In this range, the swelling pressure due to the non-uniform partitioning of mobile ions, created initially by the presence of fixed charges on the network, has been removed. The amplitude of the volume change caused by the addition of salt is a measure of the responsiveness of the network. As indicated above, one motive behind the drug-induced volume decrease is the elastic response to the reduced swelling pressure deriving from the replacement of network counterions by macromolecular drugs (proteins, micelles). Another is the attractive electrostatic forces between the network and the macromolecules. We will use the  $V/V_0$  value at 150 mM NaCl in drug-free solutions as a reference level to distinguish between those.

### 5.3. Drug – Polyelectrolyte interactions

This section evaluates a set of microfluidics experiments designed to provide information about the nature and strength of drug – polyelectrolyte interactions. After confining the microgels to traps, we first perfused PB (pH 7.4 or 5.9) through the chip to determine the equilibrium volume  $V_0$  of the microgels in a drug-free reference state. We then changed to the drug solution of choice and recorded how the microgels

developed with time. Fig. 6 shows the response of PA, HA, and DC bead microgels to PRO and Cyt C solutions, respectively. Since the solution in contact with the microgels was constantly renewed, each microgel was, in practice, in contact with an infinite volume of drug solution ("reservoir"). Under those conditions the microgel volume relaxed to a new level, with the microgels in equilibrium with the solution reservoir. The microgel volume in this state will be referred to as  $V_{\text{end}}$ .

The first section below demonstrates what information that can be extracted from the *equilibrium properties*  $V_0$  and  $V_{\text{end}}$ . After that, we demonstrate what information that can be obtained from the *kinetic properties*, i.e., the rate of change from  $V_0$  to  $V_{\text{end}}$ , and from observations of the internal structure of microgels during that process. Finally, we evaluate a rapid screening type of experiment where the setup was programmed to increase the concentration in the solution in steps at regular time intervals.

#### 5.4. Equilibrium properties

##### 5.4.1. Protein drug binding

The swelling profiles for all three microgels in PRO and Cyt C solutions (Fig. 6) show that PRO induced the largest volume decrease over the experimental time span. The result agrees with equilibrium data from the literature (Jidheden and Hansson, 2016; Johansson and Hansson, 2010; Kabanov et al., 2004; Zezin et al., 2002; Karabanova et al., 1995) and can be attributed to the difference in protein net charge (Table 2). Fig. 7A shows swelling isotherms calculated from theory ( $p = 20; q = 1; C_p^* = 2 \text{ M}$ ) for microgels in equilibrium with solutions of spheres ( $r_s = 1 \text{ nm}$ ) of opposite charge to the network and 5 mM salt. The gel volume per moles of network charges ( $n_p$ ) is plotted vs. the concentration of spheres in the solution for spheres of different charge numbers. Fig. 7B shows the corresponding binding isotherms, where  $\beta$  is the loading level expressed as protein/network charge ratio. Clearly, a protein with charge number + 21 (PRO) is expected to give rise to a much larger network contraction than a protein with charge number + 7 (Cyt C) at a given protein concentration in the solution. The calculations also show that a protein with charge number + 21 is expected to have reached the maximum drug loading level at the lowest concentration in the experiments with PA in Fig. 6A, explaining why  $V_{\text{end}}$  did not change when the concentration increased from 10 to 250  $\mu\text{M}$ . For PA + Cyt C,  $V_{\text{end}}$  increased with increasing concentration in the investigated range (Fig. 6B). This agrees with results from a previous study employing the micropipette technique (Jidheden and Hansson, 2016), where a minimum in microgel volume was observed at  $\beta \approx 0.8$ . The effect can be attributed to excluded-volume repulsion between the protein molecules, as shown by theoretical calculations with a more advanced version of the gel model (Jidheden and Hansson, 2016). This can also explain the minimum in the swelling curve at 250  $\mu\text{M}$  Cyt C in Fig. 6B since it is likely that the final loading level at this concentration exceeded 0.8.

To increase the sensitivity of the method, experiments in Fig. 6 were carried out in a medium with ionic strength lower than the physiological ionic strength. The interaction with the polyelectrolytes in the ECM will be more screened by the electrolytes present in the interstitial fluid. However, the effect will be quantitative rather than qualitative. Furthermore, investigations at low ionic strength are relevant for understanding the interactions taking place at the interface between the tissue and formulations, since proteins are often formulated at low ionic strength in order to increase the colloidal stability.

For HA microgels, it is clear from Fig. 6C-D that PRO caused a much larger volume contraction than Cyt C at 10  $\mu\text{M}$  protein in the solution. Increasing the PRO concentration did not significantly change  $V_{\text{end}}$ . For Cyt C, the volume decreased substantially as the concentration was increased to 50  $\mu\text{M}$ . The results show that for PRO, the maximum loading level was reached well below 10  $\mu\text{M}$ , but for Cyt C, the loading level increased progressively in the investigated concentration range. Fig. 6E-F show that the differences remained for their interactions with

DC beads. The results were qualitatively similar to those obtained with PA. Thus, PRO produced the largest volume change, and both proteins reached substantial loading levels already well below 10  $\mu\text{M}$ . Furthermore,  $V_{\text{end}}$  for Cyt C increased significantly as the concentration increased from 10 to 250  $\mu\text{M}$ , suggesting an excluded volume effect similar to that in PA microgels. (Careful inspection shows that also PRO gave rise to a similar but smaller re-swelling of DC beads and HA microgels whereas this was not observed for PA microgels.).

The  $V_{\text{end}}/V_0$  ratios determined for the different systems are presented in Table 3. Each entry is based on an average of eight microgels. The comparison shows that PRO interacts stronger than Cyt C, based on a lower  $V_{\text{end}}/V_0$  ratio for PRO with all three networks investigated. This can be explained by PRO's higher charge number (cf. Fig. 7). One major factor behind the effect is that the gain in entropy from replacing the network counterions with protein increases dramatically with the charge number of the protein (Johansson et al., 2010). This has a considerable effect on the concentration of protein in the solution in equilibrium with a gel and thus largely determines in which concentration range the major volume change occurs. In principle, the effect does not require direct contact between the protein and the polyelectrolyte chains. However, the attraction increases with increasing charge density on both, and will, in such cases, increase the driving force for protein binding to gel. Apart from contributing to the shift of the swelling isotherms to lower concentration, the attraction will increase the negative slope of the isotherms and can give rise to a volume phase transition (VPT) from the swollen to a much-collapsed state (cf. Fig. 7). The very low  $V_{\text{end}}/V_0$  suggests that PRO induced such a collapse in all three microgels. In contrast,  $V_{\text{end}}/V_0$  for Cyt C was considerably larger in all cases, and the protein did not induce VPT. The difference is displayed in Fig. 8, showing equilibrium swelling isotherms for HA microgels in PRO and Cyt C solutions, respectively, recorded with the microfluidic setup. Clearly, the swelling decreased gradually with the increasing concentration of Cyt C in the solution, but the microgel never reached the fully collapsed state of the PRO system. This shows that Cyt C was attracted to HA but did not form dense complex phases as did PRO.

##### 5.4.2. Amphiphilic drug binding

As a complement to the protein studies, we demonstrate that the method can also be used to study the interaction between polyelectrolytes and small self-assembling molecules, exemplified here by the cationic amphiphilic drug AMT. Fig. 9A shows a swelling isotherm for HA microgels as a function of the AMT concentration in the liquid solution. The microgel volume decreased gradually with increasing AMT concentration until just above 10 mM, where a discontinuous transition to a highly collapsed state occurred. We will let CCC (critical collapse concentration) denote the concentration in the liquid where the transition takes place. The behavior is in qualitative agreement with previous results for AMT interacting with other polyelectrolyte networks (Ahnfelt et al., 2018; Al-Tikriti and Hansson, 2020). AMT is known to form globular micelles in concentrated aqueous solutions with dimensions similar to the Cyt C molecule (Efthymiou et al., 2021). However, the micelle charge number is considerably larger than the net charge of a Cyt C molecule (cf. Table 2). This explains why the microgel volume ( $V/V_0$ ) above the CCC for AMT is comparable to  $V_{\text{end}}/V_0$  of PRO rather than Cyt C. Fig. 10 shows time profiles for the volume response of HA gels in 23 mM AMT solution. As expected, the microgel volume decreased rapidly down to the equilibrium value since the concentration was well above CCC (cf. Fig. 9A).

A discontinuity in the swelling isotherm is referred to as VPT and is predicted by the theoretical model, as shown in Fig. 9B. The model gel network is described with the same parameters as in Fig. 7A-B. The amphiphile is allowed to form spherical micelles with a radius of 1.5 nm and aggregation number 30 ( $r_s = 1.5 \text{ nm}$ ,  $Z = 30$ ). The equilibrium between micelles and free monomers is described by an equilibrium constant corresponding to the free energy of transferring a monomer between water and micelle equal to  $-7.1 \text{ kT}$ . This gives a CMC of 46 mM

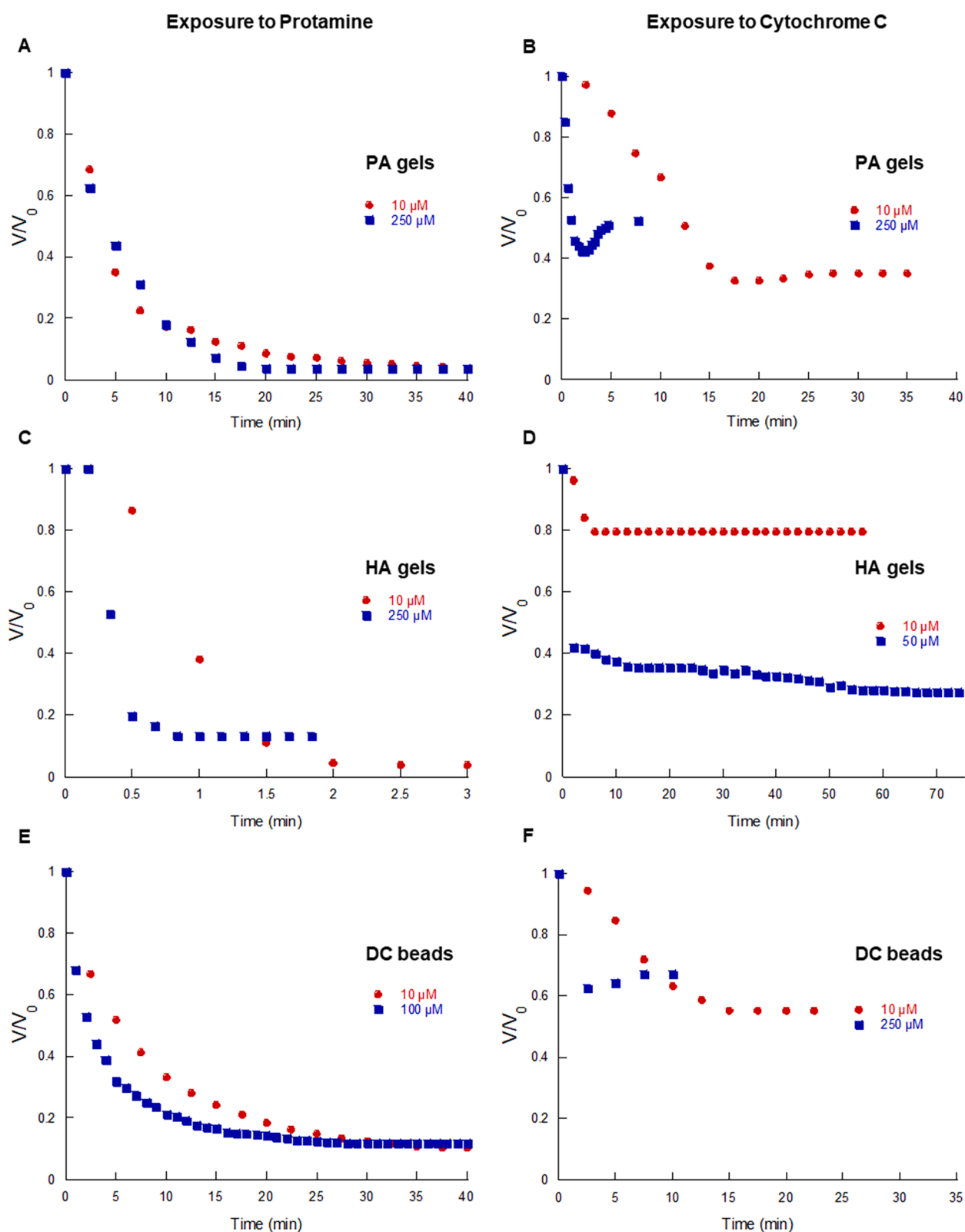


**Fig. 6.** Volume change of microgels over time when exposed to a single concentration of PRO or Cyt C in PB (pH 7.4), flow rate 200 µL/min. Each curve represents data for one microgel. **A:** PA microgel exposed to PRO (10, 250 µM) **B:** PA microgel exposed to Cyt C (10, 250 µM), **C:** HA microgel exposed to PRO (10, 250 µM), **D:** HA microgel exposed to Cyt C (10, 50 µM), **E:** DC bead exposed to PRO (10, 100 µM), **F:** DC bead exposed to Cyt C (10, 250 µM). Results presented here correspond to one microgel for each experiment.

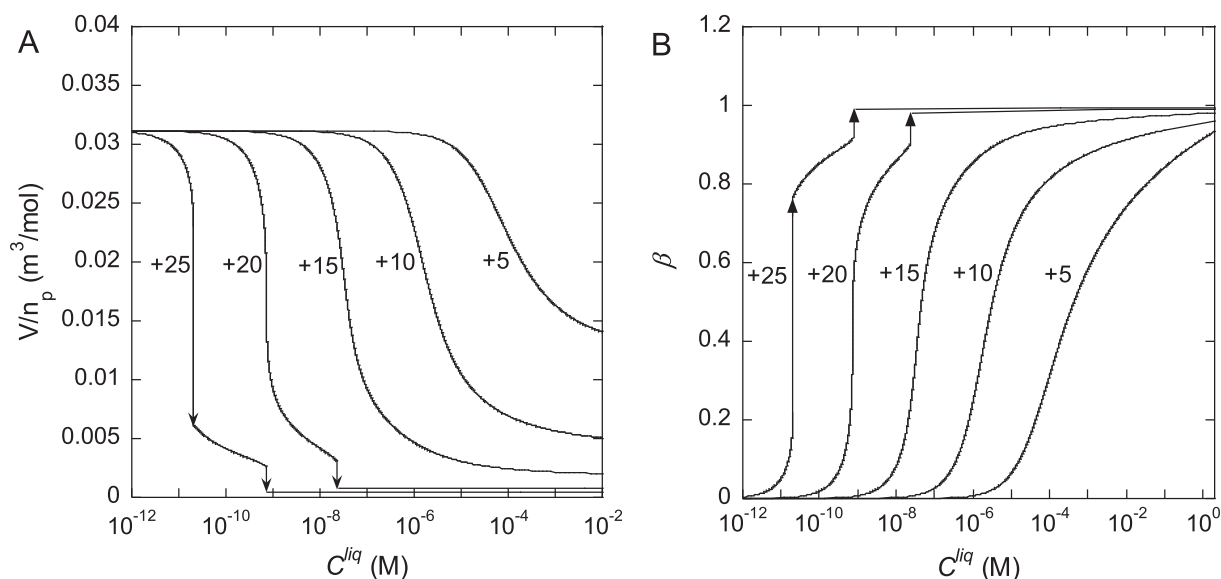


**Fig. 7.** Impact of sphere charge on swelling isotherms. Volume per amount of network charges ( $V/n_p$ ) (A) and protein/network charge ratio ( $\beta$ ) (B) plotted vs. the concentration of spheres in the liquid for different sphere charge numbers (indicated). Arrows highlight volume phase transitions (VPT) between swollen and collapsed homogeneous states.

**Table 3**  
Equilibrium microgel data<sup>a</sup>.

	$V/V_0$ <sup>b</sup>	$V_{end}/V_0$ <sup>c</sup>		
	0.15 M NaCl	Cyt C	PRO	AMT
PA	0.35 ( $\pm 0.015$ )	0.49 ( $\pm 0.016$ )	0.042 ( $\pm 0.0025$ )	0.05 <sup>d</sup>
DC	0.48 ( $\pm 0.0060$ )	0.61 ( $\pm 0.020$ )	0.13 ( $\pm 0.0022$ )	0.16 ( $\pm 0.014$ )
bead				
HA	0.46 ( $\pm 0.016$ )	0.20 ( $\pm 0.032$ )	0.051 ( $\pm 0.012$ )	0.040 ( $\pm 0.0039$ )
	$C_p$ (M) <sup>e</sup>	$C_p^{end}$ (M) <sup>f</sup>		
	0.15 M NaCl	Cyt C	PRO	AMT
PA	0.26	0.18	2.1	1.8 <sup>d</sup>
DC	0.12	0.098	0.48	0.38
bead				
HA	0.044	0.075	0.29	0.37
		$C_m^{end}$ (M) <sup>g</sup>		
		Cyt C	PRO	AMT
PA		0.026	0.10	0.045 <sup>d</sup>
DC		0.014	0.023	0.0096
bead				
HA		0.011	0.014	0.0094

<sup>a</sup> Average values of eight microgels if not stated otherwise.

<sup>b</sup> Relative microgel volume in PB (pH 7.4) + 0.15 M NaCl (no drug) after 10 min exposure.

<sup>c</sup> Relative microgel volume in the collapsed state after drug binding.

<sup>d</sup> Value for one microgel taken from (Al-Tikriti and Hansson (Al-Tikriti and Hansson, 2020)).

<sup>e</sup> Polyelectrolyte charge concentration in microgel in PB (pH 7.4) + 0.15 M NaCl (no drug) after 10 min exposure.

<sup>f</sup> Polyelectrolyte charge concentration in microgel in the collapsed state after drug binding.

<sup>g</sup> Concentration of drug substance or micelles in the collapsed state after drug binding.

within the model, which is close to the CMC of AMT (Efthymiou et al., 2021). The plot shows swelling isotherms for four different salt concentrations. At 5 mM salt (relevant for comparison with the data in

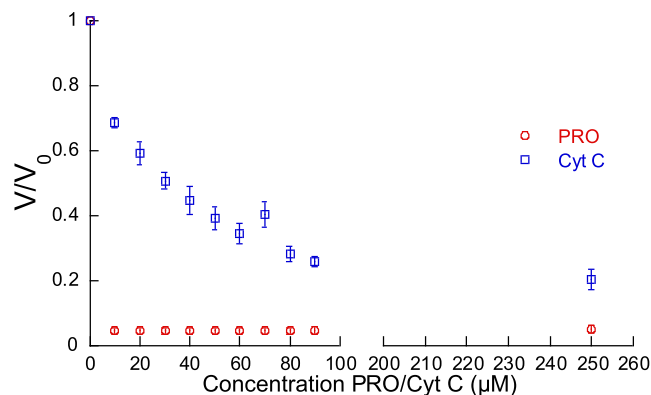


**Fig. 8.** Volume ratio ( $V/V_0$ ) of HA microgels exposed to PRO or Cyt C at different concentrations in PB (pH 7.4) (average values of eight gels). Flow rate: 200  $\mu$ L/min at 10–90  $\mu$ M and 80  $\mu$ L/min at 250  $\mu$ M.

Fig. 9A), the gel volume starts to decrease sharply at a specific concentration in the solution. This is where micelles begin to form in the gel, defined as the critical aggregation concentration (CAC). The more abrupt onset of shrinking compared to the binding of spheres in Fig. 7A reflects the cooperativity involved in the process. Although the micelle has a larger charge number than the spheres in Fig. 7A, CAC is much larger than the free concentration of spheres. This is simply because we have plotted the total amphiphile concentration on the x-axis rather than the concentration of free monomers. (Recall that micelles do exist in the solution below CMC, albeit at very low concentrations). The swelling isotherm soon reaches the point where the bulk modulus vanishes, and the gel undergoes a VPT with a large amplitude. This takes place at the CCC, where the polyelectrolyte-mediated attraction between the micelles overcomes the entropic resistance to phase transformation (Gernandt and Hansson, 2015). It is essential to distinguish between CAC and CCC to highlight that the latter does not coincide with the onset of micelle formation in the gel.

#### 5.4.3. Drug and polyelectrolyte concentration in microgel

The results presented above show that it is straightforward to rank the drug molecules after increasing binding strength to a given microgel

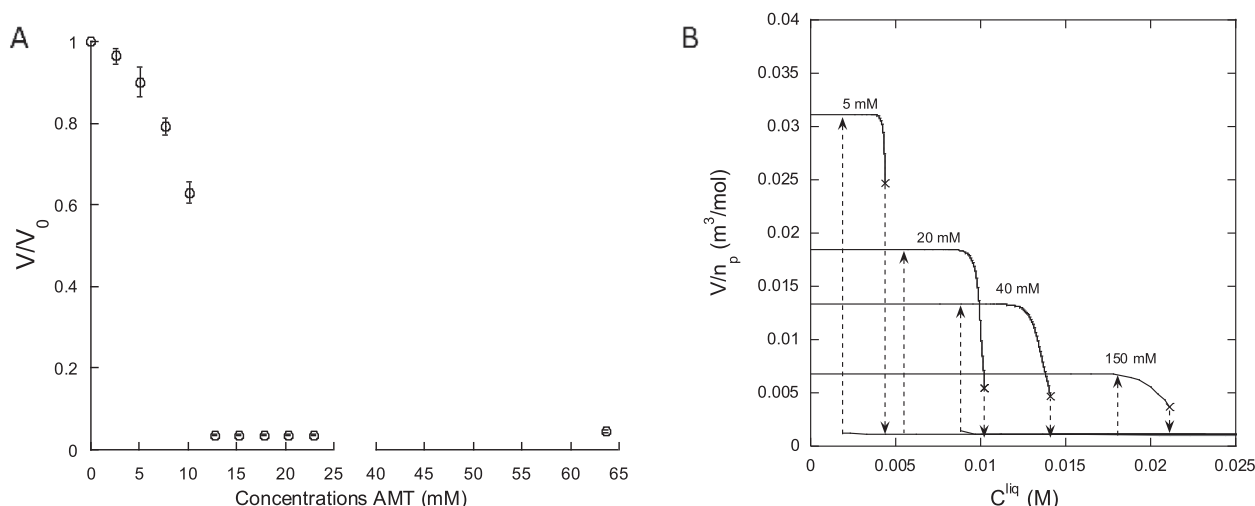


**Fig. 9.** A: Volume ratio ( $V/V_0$ ) of HA-microgels at different concentrations of AMT in PB (pH 5.9). Flow rate 200  $\mu\text{L}/\text{min}$  at 0–22.9 mM and 80  $\mu\text{L}/\text{min}$  at 63.7 mM. Average of 8 microgels presented. B: Theoretically calculated swelling isotherms for microgels in a solution of an amphiphile forming micelles ( $Z=+30$ ) in the network. Volume per amount of network charges ( $V/n_p$ ) is plotted vs. the concentration of amphiphile in the liquid ( $C^{liq}$ ) for different salt concentrations (indicated). Arrows highlight collapse and swelling transitions between homogeneous states.

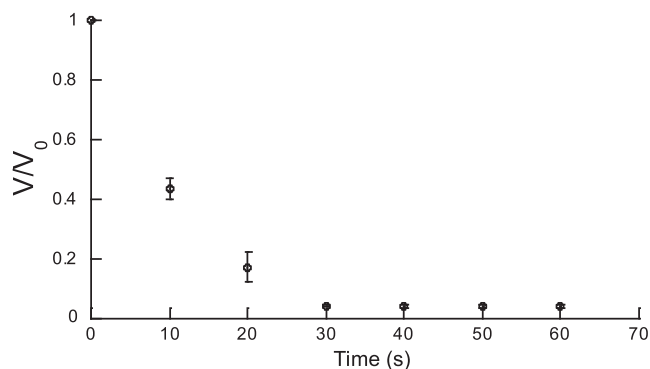


**Fig. 10.** Volume change of eight different HA microgels exposed to 22.9 mM AMT in PB (pH 5.9). Flow rate 200  $\mu\text{L}/\text{min}$ .

based on  $V_{\text{end}}/V_0$  values. For example, we have Cyt C < PRO < AMT (micelle) for binding to HA microgels, following the order of increasing charge number. However, equilibrium swelling data can also be used to rank the microgel networks based on their strength of interaction with a given drug. Here, it would be most informative to compare swelling isotherms showing  $V/V_0$  as a function of the protein concentration in the solution (cf. Fig. 8). However, for highly charged proteins, such as PRO, the binding may start at very low concentrations (cf. Fig. 7A), making it practically difficult to establish isotherms that cover the full dynamic range. Here, we focus instead on the information obtained from the comparison of  $V_{\text{end}}/V_0$  values. Since  $V_0$  is determined by several factors, including linear charge density, degree of crosslinking, and polymer concentration in the state where the network was created, it is essential to convert  $V_{\text{end}}/V_0$  into a quantity showing the density of the end state. Here we used the concentration of network charges in the reference state  $C_0$  (Table 1) to calculate the concentration of network charges  $C_p^{\text{end}} (= C_0 V_0 / V_{\text{end}})$  and the concentration of protein molecules and micelles  $C_m^{\text{end}} (= C_p^{\text{end}} \beta / Z)$  in the microgels in the fully collapsed (“end”) state. In all cases, we assumed  $\beta$  to be equal to unity. Previous investigations show that deviations from that value should not be larger than 15 % at the present ionic strength. (Al-Tikriti and Hansson, 2020; Jidheden and Hansson, 2016; Kabanov et al., 2004; Nilsson and Hansson, 2008; Karabanova et al., 1995) The result is given in Table 3. For comparison, we have included data for the microgels in 0.15 M NaCl solutions without

the drug present.

The  $C_p^{\text{end}}$  values followed the order PA > DC bead > HA for all three model drugs. It highlights the importance of correcting for the differences in  $C_0$ , since DC bead showed the highest  $V_{\text{end}}/V_0$  but not the lowest  $C_p^{\text{end}}$ . Second, we observed that PRO and AMT transformed the PA microgels into a very dense state. For example, the  $C_m^{\text{end}}$  value for AMT micelles corresponds to a micelle volume fraction of around 0.5, meaning that the network charge concentration in the space between the micelles was ca. 3.6 M, indicating strong interactions between the components. Theoretical investigations have revealed that, for packing densities of that magnitude, the swelling pressure from the excluded volume repulsion balanced by the attractive electrostatic force largely determines the swelling equilibrium (Andersson and Hansson, 2017; Gernandt and Hansson, 2015, 2016; Hansson, 2009; Johansson et al., 2010). As already noted, Cyt C induced a much smaller contraction of the PA network. The  $C_m^{\text{end}}$  value corresponds to a volume fraction of ca. 0.3, which is still relatively high. However, in this case, it is mainly the elastic network forces that bring the protein molecules together (Jidheden and Hansson, 2016). This explains why the network contraction induced by Cyt C loading in PB (pH 7.4) was comparable to the effect of adding 0.15 M NaCl (Table 3).

The polyelectrolyte chains in PA and DC bead microgels have the same linear charge density, and we could have expected them to behave more similarly. However, the comparatively large swelling of DC bead can be attributed to the neutral PVA chains providing an extra swelling pressure which prevents the gels from collapsing to the same extent as the PA microgels. For PRO, AMT, and Cyt C,  $C_p^{\text{end}}$  was respectively 4.6, 4.7, and 1.9 times lower for DC bead than for PA. The high values for PRO and AMT are explained by the crowded state produced by these molecules, where the introduction of PVA chains in the aqueous regions between the proteins/micelles is expected to significantly increase the swelling. For Cyt C, there is more space available, and so the effect of incorporating PVA is smaller. The same argument explains the difference between PA and HA in this respect. The lower linear charge density of HA means a higher molecular weight per charge. Thus, at a given network charge concentration, the polymer concentration in the microgel is larger for HA than for PA.

PRO induced the strongest contraction of PA and DC bead microgels. This can be attributed to a combination of strong electrostatic attractions to the network chains and the small diameter of the peptide chains, which in its extended conformation can be efficiently packed (Hansson

et al., 2012). HA microgels were more contracted by AMT than by PRO. This order reversal may be attributed to the significant difference in linear charge density between PRO and HA (“charge mismatch”).

#### 5.4.4. Effect of salt

The addition of salt destabilizes complexes between proteins and polyelectrolytes, and sufficiently large additions are expected to result in protein release. In the present method, the release is demonstrated directly by the decolorization of the microgel in case the protein is colored or fluorescent, or indirectly if the release is accompanied by microgel volume change. In the latter case, differences in the interaction strength can give rise to qualitative differences in the volume response. This is illustrated in Fig. 11, showing how the volume of HA, PA, and DC bead microgels in 250  $\mu\text{M}$  Cyt C solutions varies with the concentration of NaCl added to the solution. With no NaCl added, the microgels were compact and contained substantial amounts of protein. With increasing NaCl concentration, the HA microgels increased in volume up to a certain value, after which the volume decreased. This behavior is explained by swelling of the network during the phase where most of the protein molecules are released, followed by deswelling due to the salt effect on the swelling of charged networks (cf. Fig. 5). For PA and DC bead, the swelling decreased monotonically over the entire salt concentration range. The difference compared with HA can be explained by Cyt C binding stronger to the PA and DC bead networks, leading to a slower release of the protein as a function of salt concentration. See [supplementary material S4](#) for a theoretical modelling of the results in Fig. 11 and more results regarding the effect of salt on microgel swelling.

### 5.5. Kinetics

#### 5.5.1. Protein loading and release

The rate of volume change during binding and release provides complementary information about the strength of interaction between proteins and polyelectrolytes. However, the rate depends on both the rate of protein absorption from the liquid and the swelling response per absorbed protein molecule, processes which are generally coupled to each other. Therefore, when analyzing time-resolved deswelling profiles, care must be taken so as not to misinterpret the result. For charged proteins such as PRO and Cyt C, the interaction with the network charges slows down the transport inside the microgel, either by “immobilization” of individual molecules or by forming a dense surface phase (shell). In both cases, the molecules initially enrich in the outer gel layers. Since the ion exchange mechanism involved is local and the swelling response does not need to directly involve the entire network,

the deswelling response is fast. Therefore, the rate of protein mass transport from the bulk liquid to the microgel surface (“stagnant layer diffusion”) controls the rate of volume change at short times. Partly, this explains why the initial response rate induced by 10  $\mu\text{M}$  Cyt C is similar for PA, HA, and DC bead (cf. Fig. 6B,D,F), despite the significant differences in binding strength. When the mass transfer to the microgel is overall rate controlling, the microgel volume at short times is given by (Ahnfelt et al., 2018):

$$\frac{V(t)}{V_0} = (1 - kt)^{3/2} \quad (1a)$$

$$k = \frac{ShDCZa}{C_{p,0}R_0^2} \quad (1b)$$

$R_0$  is the initial microgel radius,  $Sh$  is the Sherwood number,  $D$  is the diffusion coefficient of the protein in the liquid,  $C$  is the protein concentration in the bulk liquid,  $C_{p,0}$  is the initial concentration of network charges in the microgel,  $Z$  is the protein charge number, and  $a$  is a constant. Equation 1 applies as an approximation when the protein concentration in the liquid in direct contact with the microgel is much smaller than  $C$  and  $V/V_0 = 1 - a\beta$ . Notably, the deswelling rate depends not only on the parameters describing the mass transport in the liquid ( $Sh$ ,  $D$ , and  $C$ ), but also on the parameters describing the network and protein. The linear dependence of the volume on  $\beta$  is often a good approximation when  $\beta$  is less than 0.5 (Jidheden and Hansson, 2016; Kabanov et al., 2004; Zezin et al., 2002; Karabanova et al., 1995). With  $R_0$  about the same for PA, HA, and DC bead, the observation that they respond equally fast to Cyt C binding thus shows that the ratio  $a/C_{p,0}$  is about the same for all. The parameter  $a$  describes the deswelling caused per protein charge. Based on the results associated with the data in Table 3,  $a$  is expected to increase in magnitude in the order  $\text{HA} < \text{DC bead} < \text{PA}$ , reflecting the order of increasing strength of interaction between protein and polyelectrolyte. However, since the volume ratio  $V/V_0$  describes the relative volume change, it is independent of  $C_{p,0}$ . Hence, the similarity of the observed volume response rates is more a coincidence. The conclusion is that the initial response rate depends on the strength of the interaction, but to use the rate to compare the strength of interaction between one protein and different polyelectrolytes, all microgels should have the same  $C_{p,0}$  and  $R_0$ .

The much faster volume response of all networks to PRO compared to Cyt C clearly demonstrates that the deswelling rate depends on the protein charge number. The fact that each PRO molecule entering the microgel carries the same charge as three Cyt C molecules provides a major contribution to the effect, but the ratio  $a/C_{p,0}$  is also of importance. In fact, for all three networks, Eq. (1) accounts well for the increase of the initial response rate when going from Cyt C to PRO, indicating that stagnant layer diffusion controls the initial rate also for PRO. However, PA and DC bead deviate from that behaviour at longer times, where the rate is slower than predicted by a stagnant layer diffusion control. This is explained by the formation of a collapsed shell with closely packed and slowly diffusing protein molecules, as exemplified by the microscopy images in Fig. 12, showing DC bead microgels before and after absorbing PRO.

Fig. 13A shows the result of a kinetic model for protein binding following the core-shell mechanism described in [supplementary materials S5](#). In the plot, the gel volume (solid curves) and the core volume (dashed curves) are displayed as functions of time. The model describes the phase transformation of the swollen core to the protein-collapsed shell for a process rate controlled by protein mass transport. The mass transport is mediated by protein diffusion through the “stagnant layer” in the liquid outside the microgel and through the shell. Model parameters were chosen to match the system PRO + DC bead in Fig. 6E. Thus, the model protein carried + 21 charges, and the diffusion coefficient in water was set to  $1 \times 10^{-10} \text{ m}^2/\text{s}$ , in agreement with experimental data for protamine sulfate (Shvarev and Bakker, 2005; Yuan et al., 2004). The upper and lower sets of curves were calculated for 10 and 250  $\mu\text{M}$

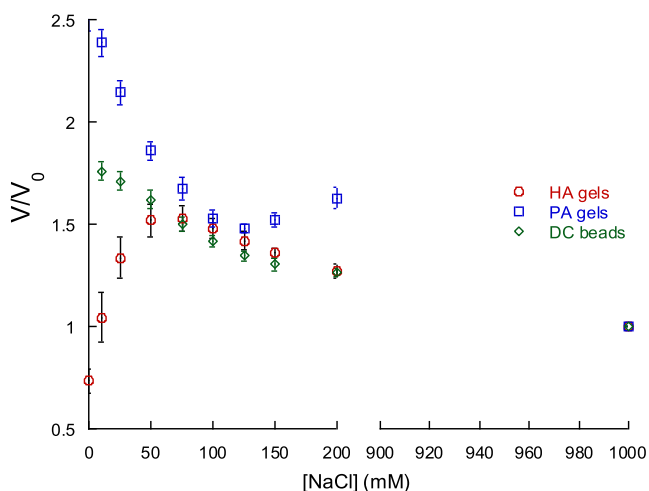
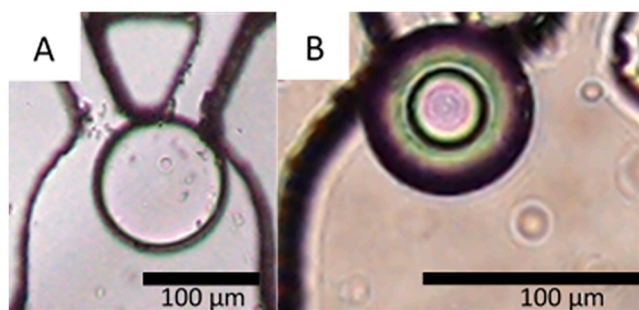


Fig. 11. Experimental results of microgel volume response at exposure to 250  $\mu\text{M}$  Cyt C at different NaCl concentrations (mean values of eight gels).



**Fig. 12.** DC beads in microfluidic traps exposed to PRO in PB (pH 7.4). **A:** Microgel with a thin shell captured early during deswelling. **B:** Microgel captured at a late state displaying a thick PRO-rich shell surrounding a swollen core. The two pictures show different microgel species. Scale bar: 100  $\mu\text{m}$ .

protein in the liquid, respectively, all other parameters were the same. The good agreement with the data in Fig. 6E allows us to draw the following conclusion from the model results. Stagnant layer diffusion controlled the initial part of the deswelling process where the shell thickness was minimal. During later stages, where the shell thickness was larger, the resistance from transport through the dense shell slowed down the process. The magnitude of the diffusion coefficient in the shell ( $3.5 \times 10^{-15} \text{ m}^2/\text{s}$ ) required for obtaining agreement between the model and the experimental data in that part indicates that the protein was immobilized by the interaction with the network. This is another indication that the PRO interacts strongly with the polyelectrolyte chains.

The same can be concluded from comparing model calculations and the experimental data for PRO's interaction with PA (cf. Fig. S8). Notably, the model calculations accounted for the timescale of the deswelling process also for PRO's interaction with the HA microgels (cf. Fig. 8). It shows that the much faster relaxation rate for HA compared with the other microgels was mainly an effect of the lower concentration of network charges in the HA microgels. However, the value of the fitted diffusion coefficient in the shell was an order of magnitude larger for HA ( $5 \times 10^{-14} \text{ m}^2/\text{s}$ ) than for the other two, in accordance with a lower protein concentration in the shell. For all microgels, the composition of the shell used in the calculation was equal to the experimental estimate for the fully collapsed state given in Table 3.

In 10  $\mu\text{M}$  protein solutions, all networks initially contracted slower in Cyt C solutions than in PRO solutions. Comparison with model calculations indicates that the initial process was rate-controlled by stagnant layer diffusion also for Cyt C, but the binding mechanism was different. The microscopy images show that the concentration of Cyt C decreased gradually from the gel border and inward. This agrees with previous confocal microscopy studies for fluorescently labeled Cyt C binding to

PA microgels (Johansson and Hansson, 2010). The latter study, although made with networks of lower crosslinking density, showed that at intermediate stages, the microgels could still be described as having a core-shell structure with much lower protein concentration in the core than in the shell. Fig. 13B shows the result of a theoretical model considering the transport through stagnant layers and diffusion of the protein in the microgel. The curves were calculated with parameters relevant for DC beads in 10  $\mu\text{M}$  Cyt C shown in Fig. 6F. Calculated curves for HA and PA are provided as supplementary material (Fig. S7), together with a derivation of the model and additional results. The model assumes that steady-state concentration gradients are maintained inside the microgel throughout the process, and that the swelling of the network at each radial distance is directly related to the local protein concentration. It only describes the process up to the point where the diffusion front reaches the center of the microgel. Local equilibrium is maintained at the microgel surface, where a Donnan type of equilibrium governs the partitioning of mobile charged species. The model makes assumptions about the distribution of material inside the microgels during the dynamic process, and therefore one should be careful not to over-interpret the results. However, our conclusion above, that the initial deswelling rate is controlled by stagnant layer diffusion is supported by the following argument. For the part of the process that the model intended to describe, it correctly reproduced the experimental deswelling rate with a diffusion coefficient similar to the literature value for Cyt C in water (Yu et al., 2019) but was found to be insensitive to the diffusion coefficient inside the microgel. Moreover, the experimental response rate was highly sensitive to the protein concentration in the liquid. The dominant role played by stagnant layer diffusion is explained in part by the fast local response rate described above and in part by the low protein concentration in the liquid, making the transport to the microgel surface slow, although the concentration in the liquid at the boundary is maintained very low throughout the process (data not shown).

To conclude, the comparison between PRO and Cyt C shows that the strength of interaction with the polyelectrolytes gives rise to detectable differences in the dynamical behavior of the microgels. In systems undergoing VPT (PRO), strong network interaction hinders the protein from redistributing in the microgel during binding. Instead, a dense surface phase (shell) grows with a sharp boundary to the core. At later stages of the process, where the boundary is detectable with light microscopy, the shell presents a significant diffusion barrier slowing down the binding and thereby the deswelling. In systems without VPT (Cyt C), where the interaction is weaker, the protein displays a diffuse concentration gradient inside the microgel during intermediate binding stages, challenging to observe with traditional light microscopy but possible to observe with confocal microscopy. In both cases, however, the deswelling rate is influenced by the rate of protein flow in the stagnant liquid

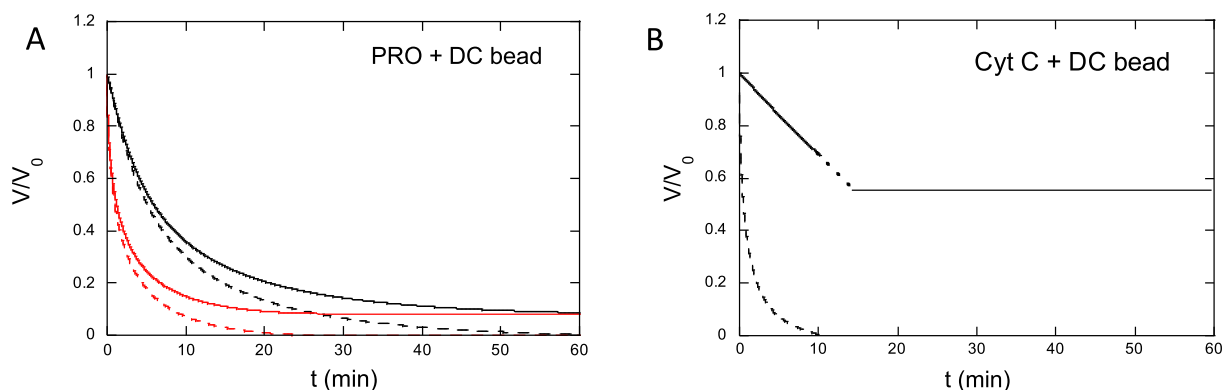


**Fig. 13.** Theoretically calculated deswelling profiles (solid curves) for DC bead in solutions of 10  $\mu\text{M}$  PRO (black) and 250  $\mu\text{M}$  (red) PRO (A), and in 10  $\mu\text{M}$  Cyt C (B). Dashed curves:  $V_{\text{core}}/V_0$ . Dotted line: Extrapolation to the region where the model is not applicable. (For interpretation of the references to colour in this figure legend, the reader is referred to the web version of this article.)

layer surrounding the microgel. The initial deswelling rate, dominated by that process, is described by Eq. (1), where the parameter  $\alpha$  (deswelling caused per protein charge) is the only factor determining the value of the “rate constant”  $k$  containing information about the strength of interaction between the protein and polyelectrolyte. Knowing the value of the other parameters,  $\alpha$  can be determined from a fit of Eq. (1) to experimental data with  $k$  as a fitting parameter.

Before ending this section, we emphasize that in all systems investigated, the initial size of the microgel affected the kinetics of deswelling but not the magnitude of the relative volume change. The larger the microgel, the larger the number of network charges, which means that large amounts of drug molecules need to bind to the microgel to reach  $V_{\text{end}}$  ( $\beta \approx 1$ ). This in turn means that it takes a longer time to reach  $V_{\text{end}}$ . For examples, see [supplementary material S6](#).

### 5.5.2. Amphiphilic drug loading and release

**Fig. 14** shows time profiles for the volume response of DC bead microgels in 0.52 mM AMT solutions in PB (pH 5.9). Qualitatively the behavior resembles that of DC bead + PRO (*cf.* **Fig. 6E**), including the core-shell phase coexistence during loading. Therefore, we have analyzed the data by means of the kinetic model used for PRO in **Fig. 13A**. We have included the result from a fit of the model in **Fig. 14**, where the solid curve is the evolution of the microgel volume and the dashed curve the evolution of the core volume. The result shows that, after a short lag period (not calculated) where the volume changed very little, the initial deswelling rate was dominated by the stagnant layer diffusion of drug monomers. This part was described by the diffusion coefficient of AMT in water ( $4 \times 10^{-10} \text{ m}^2/\text{s}$  ([Al-Tikriti and Hansson, 2020](#))). However, after  $\sim 100 \text{ s}$  the diffusion barrier presented by the shell started to influence the rate. The lower part of the deswelling curve shown was calculated with a diffusion coefficient in the shell of  $2 \times 10^{-13} \text{ m}^2/\text{s}$ . The diffusion coefficient in the shell for PRO obtained from the fit of the model in **Fig. 13A** is two orders of magnitude smaller ( $3.5 \times 10^{-15} \text{ m}^2/\text{s}$ ). The higher value for AMT can be attributed to the presence of free monomers in equilibrium with the micelles. The AMT value is of the same order of magnitude as the self-diffusion constant of dodecyltrimethylammonium chloride in the micellar cubic phase of the surfactant in water ( $5 \times 10^{-13} \text{ m}^2/\text{s}$  ([Bull and Lindman, 1974](#))). By taking the ratio of the average diffusion coefficient in the shell and the monomer diffusion coefficient in water as a measure of the fraction of free surfactant monomers in equilibrium with the micelles ([Nilsson and](#)

[Hansson, 2005](#); [Svensson et al., 2003](#)), we obtain an estimate of the free monomer concentration in the shell equal to 0.2 mM. The value agrees with the (absolute) activity of AMT at the onset of shell formation (obtained as a fitting parameter in the model). We conclude that most of the AMT molecules in the shell were effectively immobilized by the formation of micelles in complexes with the network, showing that the interaction between the drug and the polymer chains is strong. However, compared to PRO, the presence of free monomers made the AMT mass transport through the network much more efficient. Finally, we note that the kinetics of the AMT-induced collapse of HA in **Fig. 10** resembles that of AMT + DC bead. However, a theoretical analysis of data would need to take into account the simultaneous effects on the microgel volume by the increase of osmotic pressure in the liquid when adding 23 mM AMT to the solution, which is beyond the scope of the present work.

Changing the medium to PB (pH 7.4) free from AMT triggered the release of the drug. It is possible to study the kinetics and mechanism of the release process by monitoring the accompanying swelling of the microgels and their internal morphology. Results from such experiments are described in [supplementary information S7](#).

### 5.6. Verification of in vitro method as a tool for rapid screening experiments

To demonstrate that MIS can be used as a large-scale screening method for interactions between polyelectrolytes and drug substances, we carried out programmed experiments of microgels exposed to gradually increasing concentrations of either drug (loading) or NaCl (release). This allowed us to perform a large number of reproducible experiments in a short time, using less than 2 mL of drug solution for each experiment.

**Figs. 15 and 16** show examples of the deswelling of DC beads, PA microgels, and HA microgels exposed to different concentrations of PRO or Cyt C in PB (pH 7.4), where  $V_0$  is the volume of the microgels at equilibrium in PB (pH 7.4). The exposure time for each concentration was 10 min. Looking first at **Fig. 15**, it is clear that the experiment could reveal that PRO interacted stronger than Cyt C with DC bead and PA networks. However, the exposure time was shorter than the system's relaxation time at each concentration, as evidenced by the data in **Fig. 6**. Therefore, it was difficult to draw more detailed conclusions from the results. **Fig. 16** shows the corresponding data for HA-microgels. When exposed to Cyt C solutions, the microgel volume had time to relax to a new level before increasing the concentration. In this case, the conditions are better suited for rapid screening of swelling isotherms.

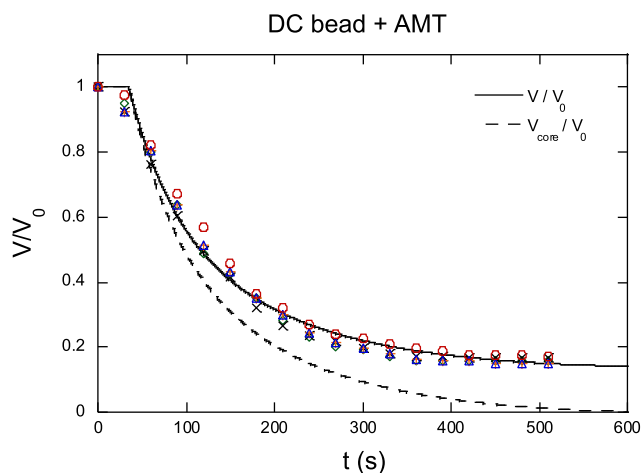


**Fig. 14.** Volume change of DC beads exposed to AMT (0.52 mM) measured in MIS over time. The total flow rate into the microfluidic chip was 200  $\mu\text{L}/\text{min}$ . Symbols: Experimental data for six different microgels. Solid curve: Theoretical deswelling profile from a fit of the kinetic model with the diffusion coefficient in the shell as fitting parameter (see text). Dashed curve: Theoretically calculated core volume.

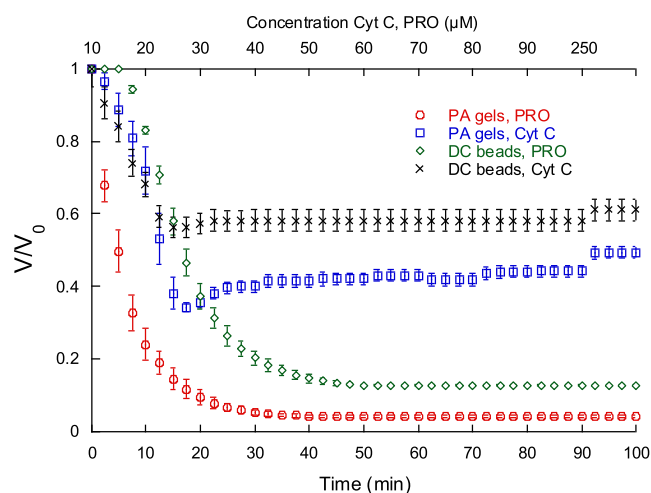


**Fig. 15.** Volume change over time for DC bead and PA microgels when exposed to Cyt C or PRO in PB (pH 7.4). Protein concentration was increased in 10 min steps starting at 10  $\mu\text{M}$  (upper x-axis), flow rate 200  $\mu\text{L}/\text{min}$  at 10–80  $\mu\text{M}$  and 80  $\mu\text{L}/\text{min}$  at 250  $\mu\text{M}$ .

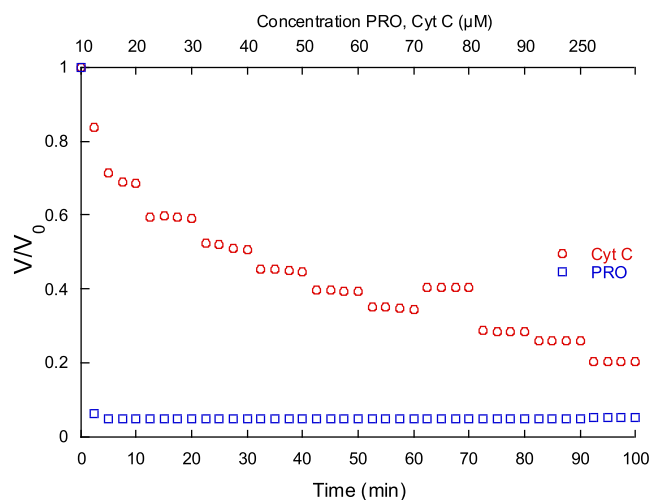


**Fig. 16.** Volume change over time for HA microgels exposed to Cyt C or PRO in PB (pH 7.4). Protein concentration was increased in 10 min steps starting at 10  $\mu$ M (upper x-axis), flow rate 200  $\mu$ L/min at 10–80  $\mu$ M and 80  $\mu$ L/min at 250  $\mu$ M.

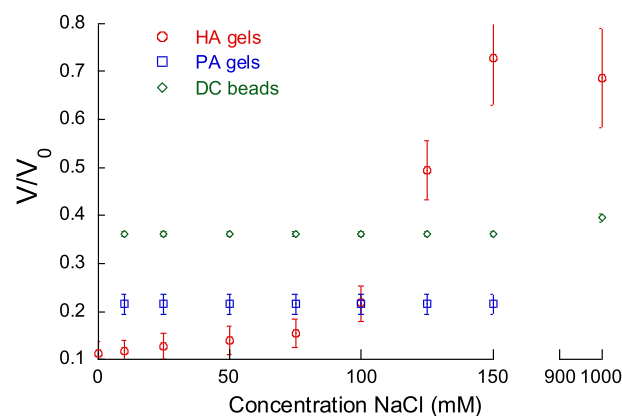
However, the level reached after exposure to 50  $\mu$ M Cyt C was slightly higher than after constant exposure to 50  $\mu$ M Cyt C (Fig. 6D), showing that longer exposure times would be needed to establish an equilibrium-swelling isotherm. With PRO, the microgel reached  $V_{\text{end}}$  already during 10 min of exposure to 10  $\mu$ M protein solutions, as expected from the data in Fig. 6E. The result shows that HA interacted stronger with PRO than with Cyt C, again demonstrating the power of the method to detect differences in the strength of interaction. HA microgels responded strongly also to AMT, but only at concentrations above the CCC, where micelles accumulated in the microgels. (Fig. S13).

Fig. 17 shows the release of PRO from DC beads, PA microgels, and HA microgels at increasing concentrations of NaCl in PB (pH 7.4). The exposure time at each concentration was 10 min, with concentrations ranging from 0 to 1 M NaCl.  $V_0$  in all these experiments is the gel volume at the highest NaCl concentration used (150 or 1000 mM), before loading the drug. Within the time frame of the experiment, no NaCl concentration tested gave any significant volume change or visual release of PRO from DC bead or PA microgels (Fig. 17). Release of PRO at 1 M NaCl from PA microgels was investigated separately and is not shown in Fig. 17. However,  $V/V_0$  after 30 min exposure to 1 M NaCl was still 0.21. In contrast, swelling of HA microgels could be detected already at 10 mM NaCl, and maximum swelling was obtained at around 150 mM NaCl, presumably corresponding to nearly complete release. However, the process caused certain damage to the microgels (data not shown), which can explain why the volume at complete release was smaller than  $V_0$  and why the final volume was different for different HA microgels in the same experiment with  $V/V_0$  ranging from 0.48 to 0.83. Results of rapid screening release experiments of Cyt C and the effect of different amount of salt in the solution during drug loading are given as [supplementary material](#) (Fig. S14–S16).

In conclusion, the results of the rapid screening release experiments clearly show that the strength of interaction increases with increasing charge density of the polyelectrolyte and charge number of the model substance, just as the single concentration experiments showed.

## 6. Conclusions

This work shows that the microfluidic chip for interactions studies (MIS) in combination with volume measurement of microgels by microscopy can be used to probe interactions between drugs and polyelectrolytes. This was demonstrated using a set of model drugs with distinctly different properties, comprising a highly charged linear peptide (PRO), a globular shaped enzyme with low surface charge density



**Fig. 17.** Volume ratio of DC beads, PA, and HA microgels during the release of PRO in PB (pH 7.4) at different NaCl concentrations. Data points are the mean values of eight microgels. Exposure time was 10 min for each concentration at flow rate 200  $\mu$ L/min for 0–150 mM NaCl, and 80  $\mu$ L/min for 1 M NaCl.

(Cyt C), and a small self-assembling amphiphilic drug (AMT). Our primary aim was to demonstrate the usability of the microfluidic method for interaction studies between components of the subcutaneous tissue and drug substances. In that context the method has advantages over existing methods developed for similar purposes, such as other gel-based methods (Leung et al., 2017; Jensen et al., 2015; Jensen et al., 2016), the micropipette-assisted method, the Scissor system (Kinnunen et al., 2015), and the HypoSkin® *ex vivo* method (Pages et al., 2018). Thus, we have shown that the method can be fully automated and can be scaled up to provide a screening tool with the capacity to probe interactions under various controlled conditions in a short time, at the same time requiring small amounts of drug samples. Furthermore, the setup of the method is modular, making it highly adaptable. In the future, the method should be suited for interaction studies between any type of polymers that can be cross-linked into spherical microgels and many classes of small and large molecules. Another potential field of application is as an *in vitro* method for controlled release which would be useful in the development of microgel-based controlled release systems.

## CRediT authorship contribution statement

**Marcus Wanselius:** Conceptualization, Methodology, Validation, Formal analysis, Investigation, Writing – original draft, Visualization, Project administration. **Sean Searle:** Methodology, Validation, Writing – review & editing, Visualization. **Agnes Rodler:** Formal analysis, Investigation, Writing – review & editing. **Maria Tenje:** Conceptualization, Writing – review & editing. **Susanna Abrahmsén-Alami:** Conceptualization, Resources, Writing – review & editing, Supervision, Funding acquisition. **Per Hansson:** Conceptualization, Methodology, Formal analysis, Writing – original draft, Visualization, Supervision, Project administration, Funding acquisition.

## Declaration of Competing Interest

The authors declare that they have no known competing financial interests or personal relationships that could have appeared to influence the work reported in this paper.

## Acknowledgments

This study is part of the science program of the Swedish Drug Delivery Center (SweDeliver) and financial support from Vinnova (Dnr 2019-00048) is gratefully acknowledged. Part of the microfabrication was performed at the SciLifeLab-Uppsala local unit Customized Microfluidics using the MyFab-Uppsala cleanroom.

## Appendix A. Supplementary material

Supplementary data to this article can be found online at <https://doi.org/10.1016/j.ijpharm.2022.121785>.

## References

- Kinnunen, H.M., Mørn, R.J., 2014. Improving the outcomes of biopharmaceutical delivery via the subcutaneous route by understanding the chemical, physical and physiological properties of the subcutaneous injection site. *J. Controlled Release* 182, 22–32.
- Patel, A., Cholkar, K., Mitra, A.K., 2014. Recent developments in protein and peptide parenteral delivery approaches. *Ther. Deliv.* 5 (3), 337–365.
- Richter, W.F., Bhansali, S.G., Morris, M.E., 2012. Mechanistic determinants of biotherapeutics absorption following SC administration. *The AAPS Journal* 14 (3), 559–570.
- Richter, W.F., Jacobsen, B., 2014. Subcutaneous absorption of biopharmaceuticals: Knowns and unknowns. *Drug Metab. Dispos.* 42, 1881–1889.
- Viola, M., Sequeira, J., Seica, R., Veiga, F., Serra, J., Santos, A.C., Ribeiro, A.J., 2018. Subcutaneous delivery of monoclonal antibodies: How do we get there? *J. Control. Release* 286, 301–314.
- Wu, Z., Hassan, D., Shaw, J.P., 2013. In-vitro prediction of bioavailability following extravascular injection of poorly soluble drugs: an insight into clinical failure and the role of delivery systems. *J. Pharm. Pharmacol.* 65, 1429–1439.
- Zou, P., Wang, F., Wang, J., Lu, Y., Tran, D., Seo, S.K., 2021. Impact of injection sites on clinical pharmacokinetics of subcutaneously administered peptides and proteins. *J. Controlled Release* 336, 310–321.
- Hagan, A., Caine, M., Press, C., Macfarlane, W.M., Phillips, G., Lloyd, A.W., Czuczman, P., Kilpatrick, H., Bascal, Z., Tang, Y., Garcia, P., Lewis, A.L., 2019. Predicting pharmacokinetic behaviour of drug release from drug-eluting embolization beads using in vitro elution methods. *Eur. J. Pharm. Sci.* 136, 104943.
- Wiig, H., Swartz, M.A., 2012. Interstitial fluid and lymph formation and transport: Physiological regulation and roles in inflammation and cancer. *Physiol. Rev.* 92, 1005–1060.
- Cooper, C.L., Dubin, P.L., Kayitmazer, A.B., Turksen, S., 2005. Polyelectrolyte-protein complexes. *Curr. Opin. Colloid. Interface. Sci.* 10, 52–78.
- Kayitmazer, A.B., Seeman, D., Minsky, B.B., Dubin, P.L., Xu, Y., 2013. Protein–polyelectrolyte interactions. *Soft Matter* 9 (9), 2553. <https://doi.org/10.1039/c2sm27002a>.
- Chan, Y.-P., Meyrueix, R., Kravtsov, R., Nicolas, F., Lundstrom, K., 2007. Review on Medusa: a polymer-based sustained release technology for protein and peptide drugs. *Expert Opin. Drug Deliv.* 4 (4), 441–451.
- Jones, A.J., Putney, S., Johnson, O.L., Cleland, J.L., 1997. Recombinant human growth hormone poly(lactic-co-glycolic acid) microsphere formulation development. *Adv. Drug Deliv. Rev.* 28, 71–84.
- Cui, F., Cun, D., Tao, A., Yang, M., Shi, K., Zhao, M., Guan, Y., 2005. Preparation and characterization of melittin-loaded poly (DL-lactic acid) or poly (DL-lactic-co-glycolic acid) microspheres made by the double emulsion method. *J. Control. Release* 107, 310–319.
- Cadée, J.A., de Groot, C.J., Jiskoot, W., den Otter, W., Hennink, W.E., 2002. Release of recombinant human interleukin-2 from dextran-based hydrogels. *J. Control. Release* 78 (1–3), 1–13.
- Kim, S.J., Hahn, S.K., Kim, M.J., Kim, D.H., Lee, Y.P., 2005. Development of a novel sustained release formulation of recombinant human growth hormone using sodium hyaluronate microparticles. *J. Control. Release* 104 (2), 323–335.
- Koten, J.W., Van Luyn, M.J.A., Cadée, J.A., Brouwer, L., Hennink, W.E., Bijleveld, C., Den Otter, W., 2003. IL-2 loaded dextran microspheres with attractive histocompatibility properties for local IL-2 cancer therapy. *Cytokine* 24 (3), 57–66.
- de Kruij, C.G., Weinbreck, F., de Vries, R., 2004. Complex coacervation of proteins and anionic polysaccharides. *Curr. Opin. Colloid. Interface. Sci.* 9 (5), 340–349.
- de Vries, R., Cohen Stuart, M., 2006. Theory and simulations of macroion complexation. *Curr. Opin. Colloid Interface Sci.* 11 (5), 295–301.
- Barroso da Silva, F.L., Lund, M., Jönsson, B., Åkesson, T., 2006. On the complexation of proteins and polyelectrolytes. *J. Phys. Chem. B* 110 (9), 4459–4464.
- Weinbreck, F., Tromp, R.H., de Kruij, C.G., 2004. Composition and structure of whey protein/gum arabic coacervates. *Biomacromolecules* 5 (4), 1437–1445.
- Kinnunen, H.M., Sharma, V., Contreras-Rojas, L.R., Yu, Y., Alleman, C., Sreedhara, A., Fischer, S., Khawli, L., Yohe, S.T., Bumbaca, D., Patapoff, T.W., Daugherty, A.L., Mørn, R.J., 2015. A novel in vitro method to model the fate of subcutaneously administered biopharmaceuticals and associated formulation components. *J. Controlled Release* 214, 94–102.
- Pages, E., Jartet, C., Descargues, P., 2018. *Ex vivo subcutaneous injection model* (Patent Application No. FR1870232). Institut National de la Propriété Industrielle.
- Bock, F., Lin, E., Larsen, C., Jensen, H., Huus, K., Larsen, S.W., Østergaard, J., 2020. Towards in vitro in vivo correlation for modified release subcutaneously administered insulins. *Eur. J. Pharm. Sci.* 145, 105239. <https://doi.org/10.1016/j.ejps.2020.105239>.
- Leung, D.H., Kapoor, Y., Alleyne, C., Walsh, E., Leithead, A., Habubliyah, B., Salituro, G. M., Bak, A., Rhodes, T., 2017. Development of a convenient in vitro gel diffusion model for predicting the in vivo performance of subcutaneous paraneural formulations of large and small molecules. *AAPS PharmSciTech* 18, 2203–2213.
- Jensen, S.S., Jensen, H., Cornett, C., Møller, E.H., Østergaard, J., 2015. Real-time UV imaging identifies the role of pH in insulin dissolution behavior in hydrogel-based subcutaneous tissue surrogate. *Eur. J. Pharm. Sci.* 69, 26–36.
- Jensen, S.S., Jensen, H., Møller, E.H., Cornett, C., Siepmann, F., Siepmann, J., Østergaard, J., 2016. In vitro release studies of insulin from lipid implants in solution and in a hydrogel matrix mimicking the subcutis. *Eur. J. Pharm. Sci.* 81, 103–112.
- Kozák, J., Rabišková, M., Lamprecht, A., 2021. In-vitro drug release testing of parenteral formulations via an agarose gel envelope to closer mimic tissue firmness. *Int. J. Pharm.* 594, 120142.
- Ahnfelt, E., Gernandt, J., Al-Tikriti, Y., Sjögren, E., Lennernäs, H., Hansson, P., 2018. Single bead investigation of a clinical drug delivery system – A novel release mechanism. *J. Controlled Release* 292, 235–247.
- Ahnfelt, E., Sjögren, E., Hansson, P., Lennernäs, H., 2016. In Vitro Release Mechanisms of Doxorubicin From a Clinical Bead Drug-Delivery System. *J. Pharm. Sci.* 105, 3387–3398.
- Al-Tikriti, Y., Hansson, P., 2020. Drug-Eluting Polyacrylate Microgels: Loading and Release of Amitriptyline. *J. Phys. Chem. B* 124 (11), 2289–2304.
- Andersson, M., Hansson, P., 2018. Binding of Lysozyme to Spherical Poly (styrenesulfonate) Gels. *Gels* (Basel, Switzerland) 4, 9.
- Andersson, M., Rasmark, P.J., Elvingson, C., Hansson, P., 2005. Single microgel particle studies demonstrate the influence of hydrophobic interactions between charged micelles and oppositely charged polyions. *Langmuir* 21, 3773–3781.
- Byssell, H., Hansson, P., Malmsten, M., 2008. Transport of poly-L-lysine into oppositely charged poly(acrylic acid) microgels and its effect on gel deswelling. *J. Colloid Int. Sci.* 323, 60–69.
- Byssell, H., Hansson, P., Malmsten, M., 2010. Effect of charge density on the interaction between cationic peptides and oppositely charged microgels. *J. Phys. Chem. B* 114, 7207–7215.
- Byssell, H., Hansson, P., Schmidtchen, A., Malmsten, M., 2010. Effect of hydrophobicity on the interaction between antimicrobial peptides and poly(acrylic acid) microgels. *J. Phys. Chem. B* 114 (3), 1307–1313.
- Hansson, P., 2020. Volume transition and phase coexistence in polyelectrolyte gels interacting with amphiphiles and proteins. *Gels* 6 (3), 24. <https://doi.org/10.3390/gels6030024>.
- Hansson, P., Byssell, H., Månsson, R., Malmsten, M., 2012. Peptide-microgel interaction in the strong coupling regime. *J. Phys. Chem. B* 116, 10964–10975.
- Jidheden, C., Hansson, P., 2016. Single microgels in core-shell equilibrium: A novel method for limited volume studies. *J. Phys. Chem. B* 120 (37), 10030–10042.
- Johansson, C., Hansson, P., 2010. Distribution of cytochrome c in polyacrylate microgels. *Soft Matter* 6 (16), 3970. <https://doi.org/10.1039/c0sm00072h>.
- Johansson, C., Hansson, P., Malmsten, M., 2009. Mechanism of lysozyme uptake in poly (acrylic acid) microgels. *J. Phys. Chem. B* 113 (18), 6183–6193.
- Nilsson, P., Hansson, P., 2005. Ion-exchange controls the kinetics of deswelling of polyelectrolyte microgels in solutions of oppositely charged surfactant. *J. Phys. Chem. B* 109 (50), 23843–23856.
- Nilsson, P., Hansson, P., 2007. Deswelling kinetics of polyacrylate gels in solutions of cetyltrimethylammonium bromide. *J. Phys. Chem. B* 111, 9770–9778.
- Gernandt, J., Hansson, P., 2012. Core-shell separation of a hydrogel in a large solution of proteins. *Soft Matter* 8 (42), 10905. <https://doi.org/10.1039/c2sm26227d>.
- Kabanov, V.A., Skobeleva, V.B., Rogacheva, V.B., Zevin, A.B., 2004. Sorption of proteins by slightly cross-linked polyelectrolyte hydrogels: Kinetics and mechanism. *J. Phys. Chem. B* 108, 1485–1490.
- Zevin, A.B., Rogacheva, V., Skobeleva, V., Kabanov, V., 2002. Controlled uptake and release of proteins by polyelectrolyte gels. *Adv. Technol.* 13, 919–925.
- Eichenbaum, G.M., Kiser, P.F., Dobrynin, A.V., Simon, S.A., Needham, D., 1999. Investigation of the swelling response and loading of ionic microgels with drugs and proteins: The dependence on cross-link density. *Macromolecules* 32, 4867–4878.
- Eichenbaum, G.M., Kiser, P.F., Shah, D., Simon, S.A., Needham, D., 1999. Investigation of the swelling response and drug loading of ionic microgels: The dependence on functional group composition. *Macromolecules* 32, 8996–9006.
- Eichenbaum, G.M., Kiser, P.F., Simon, S.A., Needham, D., 1998. pH and ion-triggered volume response of anionic hydrogel microspheres. *Macromolecules* 31, 5084–5093.
- Kiser, P.F., Wilson, G., Needham, D., 1998. A synthetic mimic of the secretory granule for drug delivery. *Nature* 394, 459–462.
- Byssell, H., Malmsten, M., 2006. Visualizing the interaction between poly-L-lysine and poly(acrylic acid) microgels using microscopy techniques: Effect of electrostatics and peptide size. *Langmuir* 22, 5476–5484.
- Byssell, H., Malmsten, M., 2009. Interactions between homopolypeptides and lightly cross-linked microgels. *Langmuir* 25, 522–528.
- Byssell, H., Månsson, R., Malmsten, M., 2011. Effects of peptide cyclization on the interaction with oppositely charged microgels. *Colloids Surf. A* 391 (1–3), 62–68.
- Byssell, H., Schmidtchen, A., Malmsten, M., 2009. Binding and Release of Consensus Peptides by Poly(acrylic acid) Microgels. *Biomacromolecules* 10, 2162–2168.
- Gernandt, J., Hansson, P., 2016. Surfactant-induced core/shell phase equilibrium in hydrogels. *J. Chem. Phys.* 144, 064902.
- Hansson, P., Schneider, S., Lindman, B., 2002. Phase separation in polyelectrolyte gels interacting with surfactants of opposite charge. *J. Phys. Chem. B* 106, 9777–9793.
- Nilsson, P., Hansson, P., 2008. Regular and Irregular deswelling of polyacrylate and hyaluronate gels induced by oppositely charged surfactants. *J. Colloid Int. Sci.* 325, 316–323.
- Björnmalm, M., Yan, Y., Caruso, F., 2014. Engineering and evaluating drug delivery particles in microfluidic devices. *J. Controlled Release* 190, 139–149.
- Andersson, M., Hansson, P., 2017. Phase Behavior of Salt-Free Polyelectrolyte Gel-Surfactant Systems. *J. Phys. Chem. B* 121, 6064–6080.
- Duffy, D.C., McDonald, J.C., Schueller, O.J.A., Whitesides, G.M., 1998. Rapid Prototyping of Microfluidic Systems in Poly(dimethylsiloxane). *Anal. Chem.* 70, 4974–4984.
- Wang, G., Li, M., Chen, X., 1997. Inverse suspension polymerization of sodium acrylate. *J. Appl. Polym. Sci.* 65, 789–794.

- Porras Hernández, A.M., Pohlit, H., Sjögren, F., Shi, L., Ossipov, D., Antfolk, M., Tenje, M., 2020. A simplified approach to control cell adherence on biologically derived in vitro cell culture scaffolds by direct UV-mediated RGD linkage. *J. Mater. Sci. - Mater. Med.* 31, 89.
- Shi, L., Wang, F., Zhu, W., Xu, Z., Fuchs, S., Hilborn, J., et al., 2017. Self-healing silk fibroin-based hydrogel for bone regeneration: dynamic metal-ligand self-assembly approach. *Adv. Funct. Mater.* 27, 1700591.
- Lewis, A.L., Gonzalez, M.V., Leppard, S.W., Brown, J.E., Stratford, P.W., Phillips, G.J., Lloyd, A.W., 2007. Doxorubicin eluting beads – 1: Effects of drug loading on bead characteristics and drug distribution. *J. Mater. Sci. - Mater. Med.* 18, 1691–1699.
- Hansson, P., 2009. Surfactant self-assembly in oppositely charged polymer networks. *Theory. J. Phys. Chem. B* 113, 12903–12915.
- Karabanova, V.B., Rogacheva, V.B., Zevin, A.B., Kabanov, V.A., 1995. Interaction of cross-linked sodium polyacrylate with proteins. *Polym. Sci.* 37, 1138–1143.
- Efthymiou, C., Bergström, L.M., Pedersen, J.N., Pedersen, J.S., Hansson, P., 2021. Self-assembling properties of ionisable amphiphilic drugs in aqueous solution. *J. Colloid Interface Sci.* 600, 701–710.
- Hansson, P., 2006. Interaction between polyelectrolyte gels and surfactants of opposite charge. *Curr. Opin. Colloid Interface Sci.* 11 (6), 351–362.
- Gernandt, J., Hansson, P., 2015. Hysteresis in the surfactant-induced volume transition of hydrogels. *J. Phys. Chem. B* 119, 1717–1725.
- Wall, F.T., Flory, P.J., 1951. Statistical thermodynamics of rubber elasticity. *J. Chem. Phys.* 19, 1435–1439.
- Hansson, P., 2009. Phase behavior of aqueous polyion-surfactant ion complex salts: A theoretical analysis. *J. Colloid Int. Sci.* 332 (1), 183–193.
- Johansson, C., Gernandt, J., Bradley, M., Vincent, B., Hansson, P., 2010. Interaction between lysozyme and colloidal poly(NIPAM-co-AAc) microgels. *J. Colloid. Int. Sci.* 347, 241–251.
- Shvarev, A., Bakker, E., 2005. Response Characteristics of a Reversible Electrochemical Sensor for the Polyion Protamine. *Anal. Chem.* 77, 5221–5228.
- Yuan, Y., Wang, L., Amemiya, S., 2004. Chronoamperometry at Micropipet Electrodes for Determination of Diffusion Coefficients and Transferred Charges at Liquid/Liquid Interfaces. *Anal. Chem.* 76, 5570–5578.
- Yu, M., Silva, T.C., van Opstal, A., Romeijn, S., Every, H.A., Jiskoot, W., Witkamp, G.-J., Ottens, M., 2019. The Investigation of Protein Diffusion via H-Cell Microfluidics. *Biophys. J.* 116, 595–609.
- Bull, T., Lindman, B., 1974. Amphiphile Diffusion in Cubic Lyotropic Mesophases. *Mol. Cryst. Liq. Cryst.* 28, 155.
- Svensson, A., Topgaard, D., Piculell, L., Söderman, O., 2003. Molecular self-diffusion in micellar and discrete cubic phases of an ionic surfactant with mixed monovalent/polymeric counterions. *J. Phys. Chem. B* 107, 13241–13250.